

Published in final edited form as:

*Langmuir*. 2010 June 1; 26(11): 8061–8074. doi:10.1021/la904481d.

## STABILITY OF AQUEOUS FILMS BETWEEN BUBBLES:

### Part 1: The effect of speed on bubble coalescence in purified water and simple electrolyte solutions

**Vassili V. Yaminsky<sup>+</sup>, Satomi Ohnishi<sup>+</sup>, Erwin A. Vogler<sup>#</sup>, and Roger G. Horn<sup>+,♦,\*</sup>**

<sup>+</sup>Ian Wark Research Institute, University of South Australia, Mawson Lakes, SA 5095, Australia

<sup>#</sup>Department of Materials Science and Engineering, The Pennsylvania State University, University Park, PA 16802-5005

<sup>♦</sup>Institute of Research Training, Deakin University, Burwood, Victoria 3125, Australia

### Abstract

Film thinning experiments have been conducted with aqueous films between two air phases in a thin film pressure balance. The films are free of added surfactant but simple NaCl electrolyte is added in some experiments. Initially the experiments begin with a comparatively large volume of water in a cylindrical capillary tube a few mm in diameter, and by withdrawing water from the center of the tube the two bounding menisci are drawn together at a prescribed rate. This models two air bubbles approaching at a controlled speed. In pure water the results show three regimes of behavior depending on the approach speed: at slow speed ( $<1 \mu\text{m/s}$ ) it is possible to form a flat film of pure water,  $\sim 100$  nm thick, that is stabilised indefinitely by disjoining pressure due to repulsive double-layer interactions between naturally-charged air/water interfaces. The data are consistent with a surface potential of  $-57$  mV on the bubble surfaces. At intermediate approach speed ( $\sim 1 - 150 \mu\text{m/s}$ ) the films are transiently stable due to hydrodynamic drainage effects, and bubble coalescence is delayed by  $\sim 10 - 100$  s. At approach speeds greater than  $\sim 150 \mu\text{m/s}$  the hydrodynamic resistance appears to become negligible, and the bubbles coalesce without any measurable delay. Explanations for these observations are presented that take into account DLVO and Marangoni effects entering through disjoining pressure, surface mobility and hydrodynamic flow regimes in thin film drainage. In particular, it is argued that the dramatic reduction in hydrodynamic resistance is a transition from viscosity-controlled drainage to inertia-controlled drainage associated with a change from immobile to mobile air/water interfaces on increasing the speed of approach of two bubbles. A simple model is developed that accounts for the boundaries between different film stability or coalescence regimes. Predictions of the model are consistent with the data, and the effects of adding electrolyte can be explained. In particular, addition of electrolyte at high concentration inhibits the near-instantaneous coalescence phenomenon, thereby contributing to increased foam film stability at high approach speeds, as reported in previous literature. This work highlights the significance of bubble approach speed as well as electrolyte concentration in affecting bubble coalescence.

### Keywords

liquid films; free films; aqueous films; bubble coalescence; disjoining pressure; Marangoni effect

---

\*corresponding author roger.horn@deakin.edu.au.

## 1. INTRODUCTION

Perhaps the most popularly-recognized manifestation of thin liquid films is the ordinary soap bubble with its beautiful, thickness-dependent iridescence arising from constructive and destructive interference of white light. These films comprise two opposing liquid-vapor surfaces separated by a thin “bulk” liquid phase.<sup>1-2</sup> In this case, surfactants dissolved in water adsorb from bulk solution, producing surfaces that resist coalescence and allow films to form with thickness comparable to the wavelength of light, producing interference colors; it is also possible to form stable films much thinner than this so that no colors are reflected (black films).<sup>3</sup>

In the early 20<sup>th</sup> century, explanations for film stability focused on kinetic factors (the Gibbs-Marangoni effect<sup>2</sup>), but later the emphasis shifted to the DLVO theory, highlighting the effect of equilibrium disjoining pressure contributions to thin film stability.<sup>3</sup> Films down to bimolecular thickness (Newton black films) have been exhaustively studied over the years, and results are compiled in many articles and book chapters dedicated to surface and colloid science. Ref. 3 is perhaps the most comprehensive monograph on the subject, dedicating more than 1000 pages to the subject of soap bubbles.

Thin films of pure water are much less familiar. It is commonly thought that pure water can only form transiently-stable films due to trace surfactant adsorption, as occurs in the formation of a dome film on the surface of a pool following rain droplet impact. Indeed, less than two pages of Ref. <sup>3</sup> are dedicated to pure-water films, and then only in reference to laboratory experiences of one of the authors.<sup>4,5</sup> Pure-water film stability, even if transient, is explained in terms of DLVO theory as a result of electrostatic repulsion of opposing charged surfaces that balances dispersion-force attraction. It is argued that a small negative surface charge on the air-water interface arises from preferential adsorption of hydroxyl ions<sup>6-22</sup> although there remains some dispute about this.<sup>23-25</sup>

Details of pure-water film stability may be more complicated than suggested by this simple DLVO picture. We recall in particular a discussion amongst marine scientists in the 1950s and 60s of emerging new evidence that salts inhibit bubble coalescence, in apparent contradiction to the prediction of DLVO. The puzzling observation was addressed theoretically at that time by Marrucci<sup>26</sup> (with references to the previous work therein) who revisited the possibility of Gibbs-Marangoni effects. The question resurfaces from time to time<sup>27,28</sup> and continues to be investigated, with more recent experimental observations that are still not fully explained.<sup>29-34</sup>

The literature is replete with attempts to model the drainage behavior of thin liquid films and drop or bubble coalescence (the following few references being representative rather than comprehensive). Some models have been based on consideration of Marangoni effects (inhomogeneous surface tension and Gibbs elasticity);<sup>26</sup> some on disjoining pressure;<sup>35</sup> some on viscous drag in the aqueous film between bubbles and its effect on deforming the bubble surface, generally assuming uniform surface tension and/or immobile surfaces;<sup>36-38</sup> some have considered interfacial viscoelasticity;<sup>39</sup> and some have taken various combinations of these effects.<sup>40-42</sup> In fact all of these phenomena are likely to be important, with some being predominant under particular conditions. Furthermore, all of them – inhomogeneous surface tension, disjoining pressure, hydrodynamic pressure, and interface deformation – are likely to be coupled, so that proper modeling becomes very complex, and beyond the scope of the present paper.

Any discussion involving water must also recognise that it is a singular and capricious substance showing complex behavior as a solvent. Biologically and environmentally important issues of water structure and specific ion effects have continued to attract attention for over a

century.<sup>43,44</sup> Difficulties in interpretation are no doubt exacerbated by the ease of water contamination by surfactants and oil (which introduces Marangoni drainage effects,<sup>2,45,46</sup> as discussed below), the ready adsorption of atmospheric CO<sub>2</sub> (with concomitant change in pH that affects ion adsorption), and the general difficulty of thoroughly eliminating residual ions from even rigorously distilled water.<sup>47</sup>

A simple thin film pressure balance apparatus developed in this study provides ways and means of overcoming experimental difficulties of forming thin films of pure water, and has allowed us to implement conditions under which pure water films are stable for days. We report measured disjoining pressure isotherms that are consistent with DLVO theory. Dynamic effects in draining thin films are also reported, with different behaviors observed at different approach rates. In particular, we observe a distinct transition from viscosity-controlled drainage to inertia-controlled drainage on increasing the speed of approach of two bubbles. The effects of simple electrolyte on the film stability and dynamic effects are also investigated.

In a companion article<sup>48</sup> (hereinafter referred to as Part 2) we explore the effects of evaporation and of trace impurities on film stability and dynamic thinning.

## 2. MATERIALS AND METHODS

### 2.1 Water treatment

Water was deionized by reverse osmosis (Microline, USA) and ion exchange (LiquiPure LS LBDR01202, USA) followed by distillation in an in-line, all-silica laminar-evaporation apparatus (Quartz et Silice, France). The resulting deionized/distilled water pH was about 5.8 (due to the dissolution of atmospheric carbon dioxide) and conductivity was in the range 0.5 – 1  $\mu$ S/cm. Repeated water purification procedures had no apparent affect on results obtained in the film balance described below.

### 2.2 Film balance

The Mysels-Scheludko type film pressure balance<sup>3</sup> employed in this work (Figure 1) was similar to the one adapted previously for investigation of evaporation-stabilized films of volatile organic liquids.<sup>49</sup> This apparatus allowed measurement of low disjoining and viscous-drag pressures, as well as interferometric visualisation of complex patterns of chaotic flow in turbulent liquid films resulting from Marangoni effects. A sodium lamp was used as a monochromatic light source (component 8 in Fig. 1). Film thicknesses were calculated from the reflection intensity based on a single-layer model.<sup>50</sup> High interference contrast at normal incidence permitted detection of trace surface contamination by oily organics which formed monolayer domains that significantly altered reflectivity (an organic layer a few nanometres thick on a 100 nm thick water film changed the reflectivity by ~ 1%).

Simplicity of the film-balance construction minimized the possibility of instrumentation-related contamination. As shown in Fig. 1, the balance consisted of only three components contacting water: (i) a flexible fluoroethylenepropylene tube (FEP Teflon, component 2 in Fig. 1, about 20 cm long with inner diameter 1 mm) connected directly to (ii) a borosilicate glass cylinder reservoir (component 3 in Fig.1) and (iii) the film-supporting polyethylene (PE) cylindrical ring (component 1 in Fig.1). The FEP tube and the PE ring were soaked in chloroform and ethanol to remove putative extractables and dried in a laminar flow hood. FEP tubing, PE ring, and glassware were treated with freshly-prepared chromic acid at 70°C (WARNING: Chromic acid is highly toxic. Ingestion and skin contact must both be avoided, and disposal through conventional laboratory or domestic waste is forbidden), then rinsed with copious quantities of purified water, and dried with nitrogen supplied from a liquid nitrogen evaporation tank plumbed through grease-free manifolds. Cylindrical capillary rings up to 6

mm long with 3–5 mm inner diameter were used in some experiments in order to avoid the top meniscus being pinned at the upper edge. The film plane was formed near the level of the tube inlet, about 2 mm above the bottom edge. After machining and cleaning the cylindrical rings and planar PE facets they were cured by surface-melting in a hot air stream, then subjected to a mild wet surface oxidation<sup>51</sup> to make the surface hydrophilic (so that rinsing water spread into a film without forming droplets), and were stored in clean water. Final assembly of the film balance was accomplished using annealed tweezers to avoid touching critical parts.

The FEP tube provided a low hydrodynamic resistance path between the PE ring and the control reservoir (component 3). The water reservoir was sealed with a polyethylene cap having a Luer connector for attaching an air filter which connected to a nitrogen line or a gas syringe (component 6) through a three-way valve (component 5). The inner diameter of the reservoir (~15 mm) was sufficiently large that the interface in the middle of the cylinder remained near-flat and corrections for the capillary pressure and level changes (due to transfer of small amounts of the water between the reservoir and the meniscus in the PE ring on changing height) were unnecessary.

The ring remained at a fixed position in the field of view of a reflection videomicroscope. The reservoir assembly (components 3, 5, 6) was mounted on a translation stage (component 4). The height could be changed by use of either a manual micrometric screw or a motor drive run at constant or variable speeds. The height difference between the plane of the film and the water level in the reservoir (hydrostatic height  $H$  in Fig.1) could also be independently measured with the aid of an accurately levelled micrometric xyz-travelling microscope. The upper meniscus interface, unless “pinned” at the upper edge when the ring height is significantly smaller than the diameter, traveled up and down smoothly along the cylindrical inner wall, following movement of the stage (with some delay at moderate to high speeds due to slight hydrodynamic resistance in the connecting tubing). For separated wetting menisci, the curvature radius of the upper surface is taken as equal to the supporting cylindrical ring radius,  $R_0 = R_c$ , to within secondary corrections for meniscus deformation under gravity. The bottom surface responded to pressure changes by changing curvature at fixed position, with the meniscus pinned at the bottom edge of the ring. The upper surface geometry and  $H$  do not change until the two closely approaching surfaces start to interact. When that happens the radius of curvature  $R$ , measured on the  $z$  axis of the shortest surface separation  $h$ , (Figure 2) becomes larger than the cylindrical ring radius, which is a few mm in our case. Once a flat film is formed (with radial extent  $a > 0$ ),  $H$  changes as much as the reservoir is moved. Given that the PE ring and reservoir surfaces were completely wettable and exhibited no contact angle hysteresis (which was the case for both water and NaCl solutions following the surface treatment and cleaning procedures described above), manometric pressure and surface distance/film thickness regulation were accurately reversible.

Optionally, fluid flow was controlled by lowering the reservoir with the air valve closed. Subsequent opening to atmosphere instantly created a pressure difference that forced water to drain from the ring under gravity. Flow rates (at a given pressure difference) could be further reduced using a capillary shunt (a co-axial capillary glass tube inset between the flexible FEP tube and the ring). This alternative mode of flow regulation, used in the dynamic experiments described below, resulted in asymptotic reduction of flow rate as hydrostatic equilibrium was approached and avoided transmission of the mechanical noise that might arise from motor operation of the system. A discussion of pressures at various locations, and how they are related to  $H$  and to local interfacial curvatures, is given in the Appendix.

## 2.3 Water films

Water films were formed in the PE supporting ring (component 1) in the following way. First, the glass cell (component 7) was filled with water to completely immerse the ring.

Disconnecting the system from atmosphere (by closing the 3-way valve, component 5) and depressurising the air inside with the syringe (component 6) caused inward flow of the water into the evacuated space (component 3). This method was found preferable to the alternative of filling the apparatus through the reservoir because it further assured that at the start of the measurements the purity of water in the ring was maintained. The water was entering the ring directly from the filling vessel in which the distillate had been collected, while contaminants possibly residing on inner walls of the instrument were progressively washed away from the ring where the water film was formed. This protocol was adopted as a standard procedure for studying stability depending on the age of the film. To suppress evaporation, the glass cell was sealed with either a mica sheet (punctured to permit insertion of tubing) or an airtight Teflon cover cap having a tilted window and tube inlet(s).

### 3. RESULTS AND DISCUSSION

All results presented here were obtained with the cell closed, so the atmosphere was saturated in water vapor. Table 1 presents a summary of our observations made in pure water and in NaCl solutions at various speeds of approach. These are discussed in more detail in the following sub-sections. In a separate paper (Part 2) we present various other observations made under conditions of evaporation and in the presence of trace amounts of contamination in the film.<sup>48</sup>

#### 3.1 Film stability with quasistatic thinning

**3.1.1 Equilibrium films of pure water**—We confirmed that highly-purified water does indeed form thin stable films, as reported long ago in Refs. <sup>4</sup> and <sup>5</sup>, and in contrast to the more recent reports of Yoon and co-workers <sup>52,53</sup> and Karakashev, Nguyen and co-workers.<sup>33,54</sup> In saturated water vapor, pure water films with a flattened area of several mm<sup>2</sup> (in a 10 mm<sup>2</sup> ring) were remarkably stable for long periods measured in hours or even days, as long as the hydrostatic pressure was kept constant and the surrounding vapor phase was saturated. Thin water films withstood significant mechanical disturbance without breaking. When noise was introduced into the system (by gently striking the apparatus, for example), ripples on the film surfaces were observed to settle within a second. Even after a pressure shock strong enough to induce chaotic flows in the film, the film was not ruptured and it returned to its uniform equilibrium thickness within a few seconds.

Figure 3 shows the relationship between disjoining pressure in the film (see Eqn. A6) and film thickness measured in the film balance. At distances below ~ 300 nm the low-value and low-gradient disjoining pressure exceeded the capillary pressure of a 4.3 mm-diameter wetting meniscus (68 Pa; see Appendix). This created a quasi-flat thin film whose radius  $a$  increased and thickness  $h$  decreased as the pressure difference  $\Delta p$   $gH$  increased. The mean curvature radius of the meniscus border around the film also decreased to less than the radius of the ring. Stable water films of some 100–300 nm thickness were observed, but films thinner than 50 nm were unstable under any experimental conditions explored in this work. The same observations were made in repeated experiments.

Using slow pressurization/depressurization and maintaining hydrostatic conditions by lowering or raising the stage (component 4 in Fig. 1) at speeds below 1  $\mu\text{m/s}$ , the film thickness changed reversibly with changing reservoir height. At these speeds hydrodynamic effects are negligible, and no inversion of the film surfaces' curvature (dimpling) was observed. The film, thinning or thickening as the stage was lowered or raised, had a uniform thickness over the entire film area, as evidenced by uniform reflection intensity and film color observed under white light. Film radius and thickness did not change once the stage was stopped at a given height, and were reproducible at a given  $H$  independent of the previous travel direction. On raising the stage,  $a$  reduced to zero at the same absolute position of the platform (with respect

to the ring and base) at which the film had initially formed. This absence of interaction hysteresis indicated that van der Waals (and hydrodynamic) adhesion between opposing surfaces was negligible under the measurement conditions employed and over the observed range of stable film thicknesses.

As we now discuss, the measured disjoining pressure isotherm<sup>55</sup> is consistent with DLVO theory (the solid line in Fig. 3), meaning that the observed film stability can be explained by the presence of electrical double layer (EDL) forces acting between charged air/water interfaces.

The DLVO theory states that disjoining pressure  $\Pi$  results from the sum of EDL forces and van der Waals (vdW) dispersion forces,

$$\Pi = \Pi_{EDL} + \Pi_{vdW} . \quad (1)$$

Between identical surfaces,  $\Pi_{EDL}$  is generally positive (a repulsive force) with an exponential dependence on the separation between the interacting surfaces, while  $\Pi_{vdW}$  is always negative (corresponding to attraction) with a power law dependence on separation.<sup>56,57</sup> DLVO theory accounts for the observed colloidal stability of many systems including dispersions of charged particles, and of oil drops or air bubbles in the presence of ionic surfactants which adsorb to the oil or bubble surfaces and create a substantial surface charge. Even in the absence of ionic surfactants, it is accepted that air/water and oil/water interfaces are charged negatively. The usual explanation given for this is that hydroxyl ions adsorb to the interface between water and a nonpolar medium. There is a large literature discussing experimental and theoretical evidence for the behavior of these ions at such an interface, with a widely held view amongst colloid scientists that an excess of  $\text{OH}^-$  is responsible for the negative surface charge of nonpolar media in water that has been observed in many experiments.<sup>6–22,25</sup> Interestingly, there is a body of theoretical work that suggests  $\text{H}_3\text{O}^+$  should be segregated to air/water interfaces, which is a puzzling result in light of the evidence for  $\text{OH}^-$  adsorption from colloid science experiments.<sup>22,23</sup>

The van der Waals component is given by

$$\Pi_{vdW} = \frac{-A}{6\pi h^3} , \quad (2)$$

in which  $A$  is the Hamaker constant. More correctly, if retardation effects are taken into account,  $A$  is not a constant but is itself a function of  $h$ . The Hamaker function  $A(h)$  can be calculated from Lifshitz theory if the dielectric properties of the interacting materials are known over a wide frequency range.<sup>58</sup> Retardation is important for  $h$  greater than a few nm, and so for the present purposes a full Lifshitz calculation has been made using the numerical method of Grabbe<sup>59</sup> and the dielectric representation of water given by Parsegian.<sup>60</sup> The results are shown in Figure 4, giving the Hamaker function (Fig. 4a) and the magnitude of the van der Waals component of disjoining pressure (Fig. 4b) as a function of aqueous film thickness. From Fig 4(a) it is seen that the simple Hamaker constant model without retardation overestimates the van der Waals attraction by a factor of about 4 at  $h \sim 50$  nm.

For the comparatively thick films observed in these experiments it is adequate to use the weak overlap approximation to calculate double-layer pressure, which results in the well-known expression<sup>56,57</sup>

$$\Pi_{EDL} = \Pi_0 \exp\{-\kappa h\}, \quad (3)$$

in which, for a simple 1:1 electrolyte,  $\Pi_0 = 64kT\rho_\infty \tanh^2(e\psi_0 / 4kT)$  and  $\kappa$  is the Debye-Hückel parameter  $\kappa = (2\rho_\infty e^2 / \epsilon\epsilon_0 kT)^{1/2}$  whose inverse (the Debye length) gives the exponential decay length of this component of disjoining pressure. In these expressions  $k$  is the Boltzmann constant,  $T$  is temperature,  $e$  is the electronic charge,  $\psi_0$  is the surface potential,  $\epsilon$  is the dielectric constant of water,  $\epsilon_0$  is the permittivity of free space, and  $\rho_\infty = 2000N_A c$  is the concentration expressed in ions/m<sup>3</sup>, with  $N_A$  being the Avogadro number and  $c$  the electrolyte concentration in mol/L.

The experimental data in Fig. 3 are fitted by a calculated DLVO disjoining pressure isotherm using a moderate surface charge ( $-0.32$  mC/m<sup>2</sup>, corresponding to a surface potential of  $-57$  mV) on the air/water interfaces, and with a Debye length of  $152$  nm which is a reasonable value for distilled water, corresponding to a 1:1 electrolyte concentration of  $4 \times 10^{-6}$  mol/L. Of this,  $1.6 \times 10^{-6}$  mol/L is attributable to  $H^+$  and  $HCO_3^-$  from dissolved  $CO_2$  which (as noted in Section 2.1) reduced the pH to 5.8. The van der Waals pressure is negligible at the measured film thicknesses of  $\sim 150$  nm or more (See Fig. 4(b)), and the film is stabilised solely by EDL forces.

In passing, we note that air is a nonpolar “hydrophobic material” with a water contact angle of  $180^\circ$ . Our experiments show no indication of any long-range attraction of the kind that has been reported in aqueous solutions between hydrophobic solid surfaces, or solids rendered hydrophobic by surfactant adsorption or other surface treatments.<sup>61</sup> Measurements of disjoining pressure between mica and mercury in water also gave no indication of unconventional long-range attraction.<sup>62,63</sup> There is mounting evidence that the so-called hydrophobic force is a capillary effect when two phases (e.g. water and water vapour or air) are present in the supporting fluid.<sup>64</sup> Our results are consistent with the view that there is no new type of force existing between hydrophobic surfaces, and there is no need to invoke a “hydrophobic force” to explain the behavior of thin aqueous films.<sup>53,54</sup>

**3.1.2 Destabilisation of film by electrolyte**—When even small amounts of NaCl were added to the aqueous films, it became impossible to produce stable films on quasi-static approach (approach speeds of less than  $1 \mu\text{m/s}$ ). At NaCl concentrations from  $0.1$  to  $0.5$  mM, marginal film stability was sometimes observed, but not consistently. At concentrations of  $0.8$  mM or more, the two menisci approached without significant deformation, and coalescence occurred at the central axis  $r = 0$  once the thickness at this point decreased to about  $50$  nm. Coalescence at “point contact” was practically instantaneous; the process could not be visually followed and explicitly resolved on a video record at  $25$  frames/s.

This result is readily explained by DLVO theory. On addition of electrolyte, a shorter Debye length reduces the range of EDL forces. At the experimental concentration of  $0.8$  mM the double-layer force corresponding to the same surface charge results in only a very weak maximum at a separation of  $\sim 40$  nm (see Fig. 3). The height of the pressure maximum is well below the experimental capillary pressures which are typically  $10$ – $100$  Pa, so that it is not strong enough to stabilise the film. Van der Waals forces begin to be effective at film thicknesses of a few tens of nm, and so the film is predicted to collapse when it thins to  $\sim 30$ – $50$  nm. This is what we observe in the experiments for all solution conditions except fresh distilled water on quasi-static approach, in which case the double-layer pressure prevents them from thinning below  $100$  nm. As previously noted by Manica et al.<sup>38</sup>, film instability can be accounted for solely by van der Waals thinning forces, without any need to invoke capillary waves or thickness fluctuations.

## 3.2 Film drainage effects at intermediate approach speed

**3.2.1 Measured film lifetime dependence on approach speed**—Now we consider dynamic experiments conducted with the alternative method of varying film thickness by opening an air valve after lowering the reservoir to a position  $H$ , as described in the final paragraph of Section 2.2, or by rapidly moving the reservoir down to a given position at the start of the measurement. In either case, water drained out of the ring while  $H$  was maintained essentially constant, i.e., the stage did not move. For larger  $H$  the two meniscus surfaces would approach at a higher speed, the film area would increase faster, and the film would expand to larger equilibrium radius  $a$  in a shorter time. In this section we discuss the results obtained at speeds of approach between  $\sim 1$  and  $\sim 150 \mu\text{m/s}$ .

In the results discussed in Section 3.1.1, water films formed slowly (using a motor drive to draw the menisci together at speeds less than  $1 \mu\text{m/s}$ ) and then maintained at a given  $H$  were observed to be stable in saturated vapor. However, water films formed faster using the alternative  $H = \text{constant}$  outflow mode, were found to be unstable. These transient films collapsed, usually after their radius (and area) stopped changing on reaching hydrostatic equilibrium between the water meniscus in the ring and the reservoir. Figure 5 shows data for a number of films monitored from the instant of formation until coalescence ( $t = 0$  was defined by extrapolation of the experimental curve to  $a = 0$ ). Coalescence time (the overall lifetime of the film) was measured as the abscissa value of the final data points of the curves of Fig. 5, each taken from the last video frame obtained within 40 ms of the sudden film collapse. It is evident that increasing  $H$  gave faster initial expansion, larger final  $a$ , and reduced film lifetime.

In films that were expanded slowly (the lower curves in Fig. 5, corresponding to values of  $H$  less than  $\sim 4 \text{ mm}$ ), interferometric observations showed the dimpling phenomenon that is well known from many thin film drainage measurements.<sup>36,62,65,66</sup> Normal dimples were observed (although they were not always perfectly axisymmetric) as shown in Figure 6(a), with film thicknesses greater near the center than near the edge (the barrier rim). The dimples grew, due to inward flow of water, until reaching a certain size, after which they drained from the center in a radial direction (outward flow). The film collapsed when its thinnest part became less than  $50 \text{ nm}$ . However, for larger  $H$  when the films expanded rapidly, non-axisymmetric dimples formed and were followed by chaotic flows within the film, similar to those described elsewhere.<sup>33,48</sup>

**3.2.2 Consideration of thin film hydrodynamics and boundary conditions**—In order to discuss these results we need to consider the hydrodynamic effects involved in thin film drainage, and in particular, how they are affected by the flow boundary condition at the air/water interface. Hydrodynamic pressure  $P_{hyd}$  in a viscous thin liquid film is related to fluid velocity gradients via the Navier Stokes equation applied within the lubrication approximation,<sup>36</sup>

$$\frac{\partial P_{hyd}}{\partial r} = \eta \frac{\partial^2 v_r}{\partial z^2} \quad (4)$$

where  $\eta$  the liquid viscosity,  $v_r$  is the flow velocity in the radial direction, and  $r$  and  $z$  are cylindrical coordinates with  $z$  being perpendicular to the film (see Fig. 2). The velocity gradients across the film depend on the boundary conditions for flow, i.e. the lateral fluid velocities at the edges of the film (the air-water interfaces in this case). If the air-water interface is immobilised by surfactants the lateral velocities at the film boundaries are zero, which means there is a no-slip boundary condition. This results in a parabolic velocity profile across the film, so the profile resembles that for Poiseuille flow. On the other hand, if the interface is fully mobile (as it should be in the complete absence of surfactant) the boundary condition is very

close to pure slip. In that case there is negligible variation in fluid velocity across the film at a given thickness, and the velocity profile resembles that for plug flow.<sup>67,68</sup> It is also possible to have intermediate situations of partial mobility, partial slip, and mixed plug and Poiseuille flow. From Eqn. (4) it is apparent that Poiseuille flow is associated with higher pressure gradients than plug flow which has  $\partial v_r / \partial z \rightarrow 0$ . The magnitude of  $P_{hyd}$  is obtained by integrating (4) from large  $r$  where  $P_{hyd} = 0$ , so it is clear that higher hydrodynamic pressures result from immobile interfaces than from mobile interfaces.

The theory of thin film drainage is well-established in the Poiseuille flow regime (immobile interfaces). For a solid sphere approaching a flat solid (or for two rigid spheres) the film pressures were computed long ago by Taylor<sup>69</sup> resulting in simple expressions for hydrodynamic pressure and total drag force (see Chan and Horn<sup>70</sup> for a derivation). For deformable fluid/fluid interfaces with immobile surfaces, numerical solutions have been developed by a number of authors, for example Refs. 36–38. Yiantsios and Davis<sup>71</sup> and Abid and Chesters<sup>68</sup> have examined thin film drainage between deformable drops with finite fluid viscosity in both the film and the drops, a situation that gives rise to partially mobile interfaces. The case of two fully-mobile fluid surfaces approaching each other, which is expected for two air bubbles in the absence of surface-active solutes, has not received so much attention. This plug flow situation has been modelled by Chesters and Hofman<sup>72</sup> who show that for mobile interfaces, film drainage is dominated by inertial rather than by viscous effects. Under these conditions the resistance to thin film drainage is much reduced,<sup>28</sup> and there is only a very small delay before coalescence occurs between two drops approaching at constant speed. Another paper by Davis, Schonberg and Rallison<sup>67</sup> has examined the case of two drops of arbitrary viscosity approaching in a viscous medium, neglecting any deformation of the drops. When the drop viscosity is small compared to the film viscosity (as in the case of air bubbles in water) Davis *et al.* show that the hydrodynamic resistance is much smaller than the classical Taylor result for immobile surfaces, being proportional to the drop (or bubble) viscosity rather than the film viscosity, and increasing less dramatically as the drops approach, with  $h^{-1/2}$  behavior rather than the well-known  $h^{-1}$  divergence of the Taylor result.<sup>69,70</sup>

From the preceding discussion, a pure, single-component liquid should have a mobile interface with air, and approaching air bubbles should collide with little hydrodynamic resistance. This is not what we have observed. However, the presence of surface-active solutes in the liquid allows the possibility of spatial variations in surface tension, which, as we discuss below, can introduce Marangoni effects. (Strictly speaking, we should speak of interfacial energies, but we will continue to use the looser term “surface tension” throughout this discussion.) Surface tension gradients tend to immobilise the liquid surface and slow the thin film drainage significantly, consistent with what we have seen experimentally at intermediate speeds of approach ( $\sim 1\text{--}150\text{ }\mu\text{m/s}$ ). As we now discuss, the Marangoni immobilisation mechanisms can be effective even for very small surface tension gradients.

Note that water can never be considered as a single-component liquid. Even in the complete absence of all solutes and impurities, the self-dissociation of water leads to the presence of hydroxyl and hydronium ions, both of which can influence the surface energy when present at or near an air/water interface. Of course surface tension will also be affected by the presence (intentional or otherwise) of other solutes including electrolytes and surface-active impurities such as trace amounts of surfactant.

Spatial variations in surface energy could be created in a number of ways when two air phases (bubbles) approach. Possible mechanisms include:

- i. The radially-outward plug flow in a thin film associated with mobile surfaces discussed in the previous section is an extensional flow that requires new surface to be created in the neighborhood of the central symmetry axis. This Gibbs or surface

elasticity effect creates a tension gradient between freshly-created surface at the center and “aged” surface remote from the center where surface-active components have had time to reach their equilibrium surface concentrations. The consequences of this effect for bubble coalescence have been discussed by Marrucci,<sup>26</sup> Prince and Blanch,<sup>28</sup> and others.

- ii. Surface flows will sweep adsorbed material along the surface, creating a concentration gradient that acts to oppose the flow.
- iii. Even if surfaces are immobile so that flow velocity is zero at the surface (no-slip), there can still be flow close to the surface which can influence the concentration of species and their effect on interfacial energy. Electrokinetic phenomena such as the creation of a streaming potential provides a familiar example in which ions in the diffuse part of an electrical double-layer are dragged along by fluid, altering the local surface potential and hence the local surface free energy.
- iv. When two charged surfaces interact through double-layer forces, the interaction can be expressed as a change in interfacial energy that is dependent on the separation between the two surfaces – the thickness of the aqueous film in the present case. The local concentrations of ions in the surface and in the diffuse double-layer also depend on film thickness. Unless the surfaces are plane-parallel, the film thickness profile is therefore associated with lateral variation of ion concentration and interfacial energy. Given that fluid flow in the film can also disturb the ion distribution due to electrokinetic effects as described in (iii), there may be a complicated coupling between local film thickness, fluid flow, ion distribution and local surface energy.
- v. Evaporation of solvent has a greater cooling effect in a thin film than in the surrounding border containing bulk fluid. This increases surface tension in the film compared to the border, driving fluid flow into the film sufficiently fast to stabilise it indefinitely, as previously demonstrated experimentally by one of us.<sup>49</sup>
- vi. Evaporation can also affect surface tension gradients by concentrating solutes in the film compared to the equilibrium concentration outside the film. This changes their adsorption at the film surfaces, creating a surface tension difference between the film and the outer meniscus. This adds another complication to the effect of evaporation on thin film behavior, which will be the subject of further discussion in Part 2.<sup>40</sup>

When any of the above effects produces a surface tension gradient along an interface, the gradient induces flow in the neighboring fluid. The lateral stress  $\partial\gamma/\partial r$  associated with inhomogeneous surface tension is balanced by tangential hydrodynamic stress at the interface  $\tau = \eta\partial v_r/\partial z$ . Some of the mechanisms that would induce a surface tension gradient are themselves associated with fluid flow (e.g. (i) – (iii) above); they create a tension gradient that opposes the original flow or “applies a brake” to it. If the surface tension gradient is sufficiently large it can arrest the tangential flow at the surface completely. This Marangoni effect is well known; for example, small quantities of surfactant can change the hydrodynamic boundary condition at a fluid-fluid interface from full or partial slip to one of no slip.

There is an interesting feature of the first of the above mechanisms for producing surface tension gradients. This mechanism requires creation of new surface area which would occur in the presence of plug flow. But if this mechanism were to produce even a small tension gradient it would immobilise the surface, whereupon new surface would no longer be created and so the mechanism would cease to operate. However, if it ceased the tension gradient would return to zero, plug flow would resume and the mechanism would be recreated. Presumably, a steady state is reached that involves a balance of plug flow creating new surface and tension gradients inhibiting the flow at the surface, leading to a situation of mixed plug and Poiseuille flow, corresponding to partial slip conditions. This balance has been discussed in the case of

flat films by Radoev et al.<sup>73</sup> and by Cain and Lee,<sup>74</sup> and in the context of bubble coalescence by Prince and Blanch.<sup>28</sup>

In the present context, the mobile boundary expected at a water/air interface could effectively be rendered partially or fully immobile if a surface tension gradient were established, for example by one of the above mechanisms. When the surface is immobile, the hydrodynamic drag resisting thin film drainage between two bubbles is significantly increased, as discussed earlier in this section. To estimate how much of a surface tension gradient would be sufficient to immobilise the aqueous film at its interfaces with air, we consider the tangential stress arising from shear in a thin film for the case of two nondeformable spheres of radius  $R_0$ . This is a familiar problem solved many years ago by Taylor,<sup>69</sup> making use of the Reynolds lubrication approximation with no-slip boundary conditions. The derivation reproduced by Chan and Horn<sup>70</sup> shows that the maximum shear stress occurs on the surface at a radial distance

$r^* = \sqrt{R_0 h/3}$ . At this position, the tangential shear stress is

$$\tau = \frac{3^{5/2}}{16} \left( \frac{R_0}{h^3} \right)^{1/2} V \eta \quad (5)$$

where  $h$  is the minimum film thickness and  $V = -dh/dt$  is the speed of approach of the spheres. To estimate the surface tension gradient required to balance this stress, suppose there is a difference  $\Delta\gamma$  in surface tension between the center of the film at  $r = 0$  and the same radial position  $r^*$ , so  $\partial\gamma/\partial r \approx \Delta\gamma/r^*$ . Equating the two tangential stresses  $\tau$  and  $\partial\gamma/\partial r$  gives

$$\Delta\gamma \approx \frac{9}{16} \frac{\eta R_0 V}{h}. \quad (6)$$

Inserting parameters appropriate to our experiment,  $\eta \approx 1$  mPa.s and  $R_0 \approx 2$  mm, shows that  $\Delta\gamma \approx 0.07$  mN/m is sufficient to fully immobilise the bubble surfaces at all film thicknesses greater than 150 nm (the range of disjoining pressure) when the approach speed is  $V \approx 10$   $\mu\text{m/s}$ . These conditions correspond to a maximum shear rate of  $7.5 \times 10^3 \text{ s}^{-1}$  at  $r^* \approx 10$   $\mu\text{m}$ .

This estimate of the variation  $\Delta\gamma$  required to immobilise the interface is likely to be an overestimate for two reasons. First, it ignores deformation of the bubbles as they approach. A more detailed calculation including deformation was made by Lin and Slattery who considered the approach of a bubble to a solid surface.<sup>37</sup> These authors assumed no-slip boundary conditions at the interface and calculated the temporal development of a dimple deformation resulting from hydrodynamic pressure built up in the thin film. Having done this, they made an *a posteriori* calculation of the surface tension difference that would balance the surface shear stress. From their modelling of Platikanov's data,<sup>65</sup> Lin and Slattery found  $\Delta\gamma \approx 0.03$  mN/m, which is less than the value estimated above from the rigid-sphere model. Comparable calculations by Manica et al.<sup>38</sup> who analyzed the drainage data of Connor and Horn<sup>62</sup> found maximal shear rates of  $\sim 10^3 \text{ s}^{-1}$  for a mm-radius mercury drop, with surfaces assumed to be immobile, approaching a mica surface at  $\sim 10$   $\mu\text{m/s}$ . This is an order of magnitude less than the shear rate that would pertain to rigid spheres, so the shear stress would be balanced by a surface tension gradient an order of magnitude less than our simple estimate. Although Connor and Horn's data was for a mercury drop approaching a flat mica surface, experimental observations in our laboratory have shown very similar scales of deformation and dimpling for an air bubble approaching mica at a comparable speed.<sup>75</sup>

A second reason for saying that Eqn. (6) gives an overestimate of  $\Delta\gamma$  is that the calculation assumed the surfaces were fully immobilised. If they were mobile, the shear gradient associated

with plug flow would be miniscule to start with, and so a smaller  $\Delta\gamma$  would start to resist the surface flow. This would generate a dynamic balance leading to partial slip and the introduction of a Poiseuille flow component, with a resulting increase in hydrodynamic pressure in the film.

The small surface tension difference ( $10^{-4}$  or  $10^{-5}$  N/m) could be caused by levels of impurity that are too low to be detected by conventional surface tension measurements. Contributions could come from adsorption of ions, including  $H^+$  and  $OH^-$  that are of course always present in water, and from local variations in structure of electrical double layers caused, for example, by an electrokinetic effect like mechanism (iii) above. The free energy of formation of a double layer is, for low values of surface potential, given by<sup>56,57</sup>

$$\Delta F = \frac{-\sigma_0\psi_0}{2} = \frac{-\epsilon\epsilon_0\kappa\psi_0^2}{2} = \frac{-\sigma_0^2}{2\epsilon\epsilon_0\kappa} \quad (7)$$

in which  $\sigma_0$  is the surface charge. Based on the parameters used in Fig. 3, this reduces the surface tension of water by  $\Delta\gamma = |\Delta F| \approx 0.009$  mN/m. This is an order of magnitude less than our simple estimate of what is required to completely immobilise an undeformed spherical bubble surface, but given the above discussion about the role of deformation and partial immobility, local variations in electrical double layer structure could create a tension gradient large enough to be a significant factor in determining the hydrodynamic boundary conditions.

At this point it is worth noting the work of Parkinson and co-workers,<sup>76,77</sup> who took considerable care to remove surface active contaminants from water by thorough purging, before measuring the rise velocity of small ( $\sim 100$   $\mu\text{m}$ ) air bubbles in bulk water and electrolyte solutions. Their results are consistent with fully-mobile interfaces,<sup>76</sup> which suggests this to be the correct boundary condition for air bubbles. Interestingly, however, the same group with the same experimental set-up found that bubbles behaved as if their surfaces were immobile as they approached a solid surface.<sup>77</sup> This suggests that a surface tension gradient can be established during thin film drainage even when the air/water interfaces are very clean, which is consistent with any of the mechanisms above (e.g. (i), (iii) or (iv)) that are associated with thin film flow and do not involve contamination.

Whatever the origin of a surface tension gradient that causes surface immobilisation, our experimental observations show film thicknesses, dimpling and transient stability that are all consistent with film thinning dominated by viscous drainage when the approach speed of  $\sim\text{mm}$  bubbles is in the range  $1\sim 100$   $\mu\text{m/s}$ .

**3.2.3 Film instability associated with viscous film drainage**—As discussed in the previous section, surface tension gradients lead to bubble flattening and dimpling, and slow down the film drainage and the speed of approach. Nevertheless, we have observed that the bubbles always coalesce after a short delay of up to  $\sim 100$  s depending on the approach speed (Fig. 5). Even at the low end of the intermediate speed range we do not observe the stable water films that were formed on quasi-static approach ( $V < 1$   $\mu\text{m/s}$ ). If positive disjoining pressure was sufficient to stabilise the films in the latter case, why is it not effective in stabilising the transient films formed when the approach speed is just a little bit higher?

A possible explanation is that instability to coalescence is associated with the phenomenon of dimpling, in which the curvature of the bubble surfaces is inverted by hydrodynamic pressure which is strongest near the axis of approach. This forms a film that has a local maximum in its thickness at  $r = 0$ , and its minimum thickness around a ring (the barrier rim) at a finite radial position  $r_b$ . Evidence for dimple formation in our experiments at intermediate approach speeds

was discussed in Section 3.2.1 (Fig. 6a); dimples did not form at approach speeds below 1  $\mu\text{m/s}$  (Section 3.1.1).

As the bubbles approach, it is clear that the surface tension near the axis must be greater than surface tension off the axis, in order to provide the surface immobilisation effect that increases hydrodynamic pressure, leading to bubble deformation and retarded thin film drainage, as discussed above. The surface tension gradient will still be present at the moment that a dimple forms, so  $\gamma_b < \gamma_c$ , where  $\gamma_c$  is the surface tension at the central axis ( $r = 0$ ) and  $\gamma_b$  is the surface tension at the barrier rim. When a dimple forms, the narrow part of the film at  $r_b$  greatly impedes the flow of water outwards from the dimple (which is why it is called a barrier). However, the surface tension gradient that is still present would act to drive flow inwards toward the center of the dimple, and indeed this is observed experimentally: the film thickness at the center increases for a time after the dimple forms, as described in Section 3.2.1.

Flow of liquid from the barrier ring toward the center of the film induced by a surface tension gradient in the same direction will cause thinning near the barrier ring, with the possibility of thinning to less than the critical rupture thickness of  $\sim 50$  nm. Another way to express this is to say that the inward flow would be associated with a negative radial gradient in hydrodynamic pressure, (Eqn. (4)) leading to the possibility of a negative hydrodynamic pressure, and the sum of hydrodynamic pressure and disjoining pressure<sup>78</sup> being less than the capillary pressure even when the disjoining pressure (discussed in 3.1.1) is slightly larger than the capillary pressure. That situation would lead to collapse of the film (see Appendix).

It is also worth noting at this point that inhomogeneities in surface tension that were not symmetric around the  $r = 0$  axis would create flows in nonradial directions, which would lead to local variations in thickness and likely film rupture at its thinnest point. Some observations and discussion of non-axisymmetric thickness variations are given in Part 2.<sup>48</sup> Asymmetric drainage of thin films has also been discussed by other authors including Joye *et al.*<sup>79</sup> and Karakashev *et al.*<sup>33</sup>

The inward (centripetal) flow effect would only be operative after a dimple forms. Before dimple formation the bubble surfaces remain convex, and liquid in the film always flows outward (centrifugally) as the bubbles approach. For this reason we suppose that coalescence can occur only after bubble flattening and dimple formation. If a dimple did not form before the film reduced to the thickness at which double-layer repulsion provided sufficient disjoining pressure to balance the capillary pressure, the film would come to a stable equilibrium.

We can estimate the separation at which bubbles flatten by calculating the hydrodynamic pressure at the center of the film and comparing it to the capillary pressure. The former is given (for spherical surfaces and no-slip boundary conditions) by<sup>70</sup>

$$P_{hyd} = \frac{3\eta R_0 V}{2h^2}. \quad (8)$$

Equating that to capillary pressure  $2\gamma / R_0$  leads to the following estimate for the separation at which the surfaces become flat:

$$h_f = \frac{R_0}{2} \sqrt{\frac{3\eta V}{\gamma}}. \quad (9)$$

This simple estimate differs by a numerical factor of about 2 from the separation at which dimpling is predicted to occur from a full numerical calculation by Klaseboer et al.,<sup>36</sup>

$$h_d = 0.4R_0 \sqrt{\eta V / \gamma}.$$

From Fig. 3 we can see that the film thickness at which double-layer disjoining pressure equals the capillary pressure of  $\sim 70$  Pa is about 150 nm. Using Eqn. (9), the approach speed that would cause flattening at this separation is  $V \sim 0.6 \mu\text{m/s}$ . According to our model, speeds less than this would allow stable flat films to form, and speeds greater than that would lead to film collapse after a certain drainage time. This is what is observed experimentally, giving evidence to support our argument that instability of transient films follows from dimple formation. Using the expression of Klaseboer et al.<sup>36</sup> for dimpling thickness leads to an estimate of  $V \sim 3 \mu\text{m/s}$ . The former value is closer to the experimental observation that stable films are formed at  $V < 1 \mu\text{m/s}$ .

The model presented here is also consistent with coalescence time decreasing as  $H$  and the speed of approach increase (Fig. 5). Higher approach speeds cause more pronounced dimples, and may also create greater surface tension gradients through mechanism (i), causing a greater ingress of water into the dimple and thus more rapid thinning at the barrier rim, leading to shorter coalescence time.

**3.2.4 Effect of electrolyte**—At NaCl concentration as low as  $8 \times 10^{-4}$  M, when the meniscus surfaces approached at a speed of several  $\mu\text{m/s}$ , the solution films began to form when their thicknesses were  $\sim 100$  nm, about 2 – 3 times thinner than those for distilled water films. Only transient stability was observed. While film radius  $a$  slowly increased with increasing  $H$ , the draining film developed characteristic cylindrical wedge asymmetry by gradually thinning somewhat faster on one side than the other, as shown by the darker area in Fig. 6(b). The wedge direction with respect to the ring varied randomly from measurement to measurement and gradually shifted during the drainage, showing that the effect is not due to the location of the drainage tube, nor to any asymmetric imperfection of the PE ring. The drainage continued without reaching equilibrium thickness  $h$  at any given hydrostatic pressure, i.e., after stopping the stage and fixing  $H$ . After a minute or so the film, which by the time of collapse was typically 10% thinner on one side than the other, ruptured once the minimum  $h$  fell below 50 nm.

The quasi-static behavior in salt solutions (Section 3.1.2) is similar to that observed for bubbles in organic liquids, which also coalesce without forming films. However, finite-speed effects are strikingly different for bubbles in organic liquids compared to those in aqueous electrolyte solutions. On increasing  $V$  above  $1 \mu\text{m/s}$  we observe formation of transient films at NaCl concentrations as low as  $8 \times 10^{-4}$  M, which is already sufficiently high that equilibrium films do not form. In contrast, no approach-speed transition to a film-formation regime is observed for bubbles in organic liquids. This is accounted for by the above discussion – the transient stability is associated with viscous film drainage and bubble dimpling that only occurs in the presence of solutes that can adsorb/desorb and create surface tension gradients. Simple electrolyte provides at least two such species in water (anions and cations), but properly purified organic liquids are free of solutes.

### 3.3 Dynamic effects on rapid approach

**3.3.1 Observation of transition to instant coalescence**—For large values of  $H$  ( $> 20$  mm), giving surface approach rates above  $\sim 150 \mu\text{m/s}$ , films did not form at all. At about this speed there appeared to be a transition to a completely different drainage behavior with the coalescence time suddenly reduced to zero (the data in this case would be represented by a single point  $t=0$ ,  $a=0$  on the graph of Fig. 5). No sign of transient film formation was observed, even though films were forming and surviving for about 10 – 20 seconds at just slightly lower

collision velocities (the upper curves in Fig. 5 have  $dh/dt$  just under  $150 \mu\text{m/s}$  at small  $t$ ). In faster collisions the two bubble surfaces (menisci), showed no sign of slowing down as they approached, and collided instantly when they met, presumably by van der Waals instability at  $h$  around  $50 \text{ nm}$ . No deformation of the menisci surfaces from their original spherical shape was observed in the interference fringes, and coalescence occurred within one video frame ( $40 \text{ ms}$ ).

The transition speed to instantaneous coalescence did not depend on the rate of evaporation of the pure water film; it was practically the same in open (with evaporation) and closed (vapor-saturated) cells. However, while we generally cite  $150 \mu\text{m/s}$  as a typical value, there was some variation in transition speed from experiment to experiment. As we will discuss in Part 2, ageing of the water film, leading to possible organic contamination of water interfaces, tends to shift the transition point to higher speeds, e.g., from  $\sim 100 \mu\text{m/s}$  in freshly-distilled water to  $\sim 200 \mu\text{m/s}$  in water that had been distilled  $\sim 12$  hours previously.<sup>48</sup>

The observation of instantaneous coalescence suggests that the mechanism responsible for film formation at slower approach speeds decreases or disappears entirely above some threshold speed. The effect could be explained if the maximum interaction pressure experienced in the film before coalescence were reduced at high speed to a value less than the capillary pressure  $2\gamma/R_c$  (see Appendix 1). Clearly, in lower-speed collisions the interaction pressures exceeded the capillary pressure, as indicated by the mere fact of forming and maintaining the films, either transiently at intermediate speeds ( $1 - 150 \mu\text{m/s}$ ) or with stability of at least hours at very low approach speeds ( $< 1 \mu\text{m/s}$ ). At first sight it seems surprising that at higher approach speeds there is less interaction pressure, considering that hydrodynamic repulsion is expected to become stronger and longer-range, not weaker, when collision velocities increase. However, there is a simple explanation, which we outline in the following section.

**3.3.2 Explanation for transition to inertial film drainage**—Clearly the maximum possible  $\Delta\gamma$  is limited in any system – it cannot exceed  $\gamma$  and in most cases it would not exceed  $\sim\gamma/2$ . This means there is a limit to the Marangoni effects' capacity to overcome flow stresses and immobilise the interface. Eqn. (5) predicts that for a given speed of approach  $V$ , the tangential shear stress associated with viscous drainage flow increases as  $h$  decreases. Eqn. (6) predicts that for a given  $\Delta\gamma$  and approach speed  $V$ , the tension gradient can be large enough to exceed the flow stress and immobilise the surface at large  $h$ , but at small  $h$  it cannot. When approaching bubbles reach the critical separation given by rearranging (6):

$$h_m \approx \frac{9}{16} \frac{\eta R_0 V}{\Delta\gamma} \quad (10)$$

their surfaces will become mobile, flow in the film will be dominated by inertial over viscous effects, hydrodynamic pressures will be greatly reduced (as discussed in Section 3.2.2),<sup>67,72</sup> and there will be little deformation and little resistance to approach of the bubble surfaces. In other words, the Marangoni “brakes” will fail on approach, and the separation at which they will fail is proportional to the approach speed.

At sufficiently high speed the transition to mobile interfaces will occur at a separation that may be too large for hydrodynamic pressures and flattening to have become significant. The result is that rapid approach continues with little hydrodynamic resistance until there is a near-instantaneous collision. This is what we have observed experimentally for speeds in excess of  $\sim 150 \mu\text{m/s}$ . Davis *et al.*<sup>67</sup> show that hydrodynamic drag between bubbles with mobile surfaces would be orders of magnitude less than that calculated for immobile surfaces (their Eqn. 16). The analysis of Chesters and Hofman<sup>72</sup> predicts that for fully mobile interfaces, dimpling starts

at a film thickness  $h^* \sim 10^{-2}$  in their dimensionless units; converting that to real units for  $\sim$ mm bubbles approaching in water at  $V \sim 100 \mu\text{m/s}$  yields an unobservably small dimpling separation,  $h_d \sim 0.1 \text{ nm}$ . Chesters and Hofman also show that coalescence occurs in this system even in the absence of attractive surface forces, after a delay time of  $t^* \sim 1$ . For our system this corresponds to  $\sim 1 \mu\text{s}$ , far below our experimental resolution. An alternative analysis of Abid and Chesters<sup>68</sup> for partially mobile surfaces takes into account fluid circulation and viscosity within dispersed drops. In this case, dimpling is observed at a (different) dimensionless  $h^* \sim 0.1$ . Putting in parameters for two  $\sim$ mm air bubbles approaching at  $100 \mu\text{m/s}$  (notwithstanding that the low viscosity of air puts this calculation on the margins of validity of their analysis) gives a dimpling separation of  $h_d \sim 1 \text{ nm}$ ; again, too small to be observed experimentally.

At lower approach speeds the surfaces would remain immobile to smaller separations (film thicknesses), allowing hydrodynamic pressures in the film to increase. This can cause deformation of the bubbles, which will first flatten and then dimple as their surfaces approach. Once bubbles flatten and dimple, the rate of approach of their surfaces is reduced in the deformed area. This has been demonstrated in detailed numerical calculations by Lin and Slattery<sup>37</sup> for immobile surfaces and by Abid and Chesters<sup>68</sup> for drops approaching at constant speed with partially-mobile surfaces. Furthermore, Lin and Slattery showed that the surface tension difference required to balance the shear stress decreases significantly after a dimple forms. This means that if bubbles start flattening while still in the immobile-surface region that pertains at large  $h$  ( $h > h_m$  given by Eqn (10)), their surfaces will *remain* immobile because the Marangoni effect is large enough to balance the decreasing flow rates and shear stresses that ensue.

To understand this more clearly, note that the critical film thickness at which bubble surfaces are predicted to undergo a change from immobile to mobile as they approach increases linearly with approach speed  $V$  (Eqn. 10), while the critical thickness for the onset of flattening and dimpling increases with  $\sqrt{V}$  (Eqn. 9). Thus for sufficiently large  $V$  the former transition will occur before flattening begins, and the bubbles will approach with mobile surfaces and negligible hydrodynamic resistance. Equating (9) and (10) allows an estimate of the critical speed  $V_c$  above which a near-instantaneous collision is predicted from these considerations:

$$V_c = \left(\frac{4}{3}\right)^3 \frac{\Delta\gamma^2}{\eta\gamma}. \quad (11)$$

Putting  $\Delta\gamma = 0.07 \text{ mN/m}$ ,  $\gamma = 73 \text{ mN/m}$  and  $\eta = 1 \text{ mPa}\cdot\text{s}$  gives an estimate of  $V_c \sim 160 \mu\text{m/s}$ , close to what was observed in our experiments. It is interesting to note that this very simple model predicts a critical coalescence speed that is independent of bubble radius.

**3.3.3 Influence of electrolyte on rapid approach**—At  $10^{-1} \text{ M}$  and higher NaCl concentrations we observed no transition back to instantaneous coalescence in the high-speed limit, not even at surface approach speeds of  $1 \text{ mm/s}$ . Transient films were formed at all speeds  $V$  above  $1 \mu\text{m/s}$ . This is an order of magnitude higher than the  $\sim 150 \mu\text{m/s}$  critical speed at which we observe instant coalescence of bubbles of similar size in distilled and low salinity water. Note that EDL repulsion is negligible at such high salt concentrations.

A mechanism of creating surface-elastic resistance and causing the coalescence delay in high-speed collisions of bubbles in electrolyte solutions was presented by Marrucci<sup>26</sup> who discussed how the flow acceleration in the process of film thinning creates fresh surface area with a different tension to the equilibrium value that pertains outside the film. Interestingly, it does not matter whether the ions (or other solute) are positively or negatively adsorbed; the effect is shown to be proportional to  $(\partial\gamma/\partial c)^2$  where  $c$  is the solute concentration. Marrucci did not

consider diffusion of ions toward the surfaces of the film, which can be rapid because the film is very thin. This has been discussed by Prince and Blanch,<sup>28</sup> who noted that the diffusion constants of different ions will play a role in determining the magnitude of their effect on surface elasticity in a given experimental situation, which provides one reason why the effect would depend on the electrolyte species. As previously shown by Christenson and Yaminsky,<sup>30</sup> the surface elasticity in an expanding thin film with rapid adsorption/desorption is also proportional to  $(\partial\gamma/\partial c)^2$ , hence also dependent on electrolyte species. However, Safouane and Langevin<sup>80</sup> have recently demonstrated that the dependence of bubble coalescence on electrolyte species does not correlate with measured surface elasticity, suggesting that elasticity is not the only factor involved. It should be noted that the model we have proposed here does not depend on any particular mechanism for the formation of a surface tension gradient, only that such a gradient can be created.

The value of  $\partial\gamma/\partial c$  for NaCl is 1.6 mN/m/M, giving an estimated  $\Delta\gamma = 0.16$  mN/m in 0.1 M NaCl. Putting this value in Eqn. (11) gives a critical speed for coalescence of about 0.9 mm/s, which, given that it is no more than a simplistic estimate, is consistent with the experimental observations. This model predicts that the critical speed would depend on the electrolyte species since these have different values of  $\partial\gamma/\partial c$ . Conversely, conducting experiments at a particular approach speed<sup>27,33,34</sup> (or flow conditions for bubble swarms<sup>29</sup>) would see some electrolytes inhibiting coalescence and others not, with a transition concentration that is specific to the electrolyte species. For example, Lessard and Zieminski<sup>27</sup> found various transition concentrations for a series of inorganic electrolytes, in an experiment in which two bubbles were pressed together at an approach speed which we estimate (from their rate of bubble volume growth) to be  $\sim 3$  mm/s. Putting this value of  $V_c$  in Eqn. (11), setting  $\Delta\gamma = c \cdot \partial\gamma/\partial c$ , and solving for  $c$  gives a predicted transition concentration of 0.19 M for NaCl, which is close to the measured value of 0.175 M. Under the experimental conditions of Ref. <sup>27</sup> contact times in the elastic bubble collisions were shorter than a second, a minor fraction of the drainage time, so the motion direction was reversed from approach to separation long before the film could thin to coalescence.

It is interesting to note that Prince and Blanch<sup>28</sup> were also successful in predicting the transition concentration observed by Lessard and Zieminski, using a model in which they examined drainage in the mobile-interface regime and asking at what salt concentration there would be a transition to immobile surfaces based on the Marrucci model,<sup>26</sup> in effect approaching the transition from the opposite side to what we have done in our model.

It was also noted in Section 3.3.1 that organic contamination of the water film increases the critical coalescence speed to higher values. This is consistent with the above discussion, since organic contamination would increase the value of  $\Delta\gamma$ .

#### 4. THREE REGIMES OF FILM BEHAVIOR

In the previous section we proposed mechanisms that can explain the experimental observations. Three qualitatively different types of behavior have been observed for bubbles approaching in purified water, at low, intermediate, and high approach speeds. The three regions of behavior are illustrated in Figure 7. Each region is defined by which of three curves shown in the figure is uppermost: Eqn. (10) (solid line) which marks the boundary between immobile and mobile interfaces for a given value of  $\Delta\gamma$ ; Eqn. (9) (dotted line) which marks the onset of flattening if the surfaces are immobile; and the horizontal dashed line showing the thickness at which disjoining pressure equals the capillary pressure.

Consider what happens if two bubbles approach from large  $h$  at a given speed. At low speed (Region I shown in Fig. 7a) the bubbles approach until they reach the separation at which the disjoining pressure stabilises a thin film. At intermediate speed (Region II) the bubbles have

immobile surfaces at large separation, giving rise to viscous drainage, and as the bubbles approach they reach the dotted line which marks the separation at which they become flattened by hydrodynamic pressure. Flattening and subsequent dimpling retards the approach of the surfaces, shear stresses are reduced, and the surfaces remain immobilised by surface tension gradients. This delays coalescence for a while, but when the film thins further it is destabilised by the tension gradient driving liquid toward the central axis to inflate the dimple, causing thinning at the barrier rim until rupture occurs. At high speed (Region III in Fig. 7b) the bubbles cross the solid line, and their surfaces change from immobile to mobile before the hydrodynamic pressure is great enough to cause flattening. With mobile surfaces, the bubbles approach with little hydrodynamic resistance (inertial drainage), do not deform, and they coalesce almost as soon as their surfaces meet.

The models used in constructing Fig. 7 are simplistic and semiquantitative at best, and we should not expect this picture to give precise values for the boundaries between different modes of film drainage. Nevertheless the models do (with one adjustable parameter) produce predictions that accord with the experimental observations reported in Section 3. The dashed line in Fig. 7 is fixed by the Debye length and bubble radius. The dotted line (Eqn (9)) is fixed by the surface tension and viscosity of water and the bubble radius. The gradient of the solid line (Eqn (10)) is sensitive to the surface tension differential  $\Delta\gamma$ . With little knowledge of what this might be, we have chosen a value of 0.07 mN/m for the curves shown in Fig. 7, and this value produces predictions for the two transition speeds  $V_{I-II}$  and  $V_{II-III}$  of 0.6 and 160  $\mu\text{m/s}$  respectively. The experimental values are about 1 and 150  $\mu\text{m/s}$ .

Now consider what happens to the transition lines in Fig. 7 on addition of electrolyte. First, the dashed line showing the range of disjoining pressure would disappear, because adding electrolyte reduces the double-layer interaction so much that it never approaches the capillary pressure (see Fig. 3). Thus Region I (stable film formation) will never occur. Second, the maximum value of  $\Delta\gamma$  will be increased because of increased Gibbs elasticity of salt solutions, which decreases the slope of the solid line (Eqn. 10) and moves the crossover between Regions II and III to higher approach speeds.

These changes are consistent with our experimental observations with added electrolyte: the behavior is consistent with Region II (bubble deformation followed by delayed coalescence) at all experimental approach speeds up to  $\sim 1$  mm/s, which is the practical limit in our film balance. The model is also consistent with other observations of bubble coalescence in which added inorganic electrolytes tend to inhibit bubble coalescence when present above a certain concentration that is specific to the electrolyte species.<sup>27,29,32,34</sup> However, the effect of approach speed has not, to our knowledge, been properly examined so far in bubble coalescence experiments involving single bubble-pairs or thin films. Previous observations of bubble coalescence have generally been done under constant experimental conditions of bubble approach or of flow fields in bubble swarms. Hence bubble approach speeds have not been controlled, although they are likely to be approximately constant for a given experimental method. The present work highlights the fact that speed may be an important parameter in bubble coalescence, which makes it problematic to compare results (e.g. critical salt concentrations) between different experiments.

Experiments involving clouds of bubbles in flows that generate higher approach speeds ( $\sim 10$  cm/s) indicate that at these speeds there may be another transition back to non-coalescence.<sup>81, 82</sup> Discussion of this effect considers deformation and dimpling when the interfaces are mobile, suggesting that when dimpling occurs in inertial flow, two bubbles may bounce apart before the film between them has time to drain to a collapse thickness.<sup>72,81,82</sup> This requires substantially higher speeds than those explored here.

Some other remarks on observed bubble behavior can be made in light of the model presented here. The viscous drainage period (Region II) explains why  $R = 1 - 2$  mm air bubbles rising under buoyancy in salty or impure water stay at the solution surface for several seconds before bursting; this common "non-DLVO" observation that inspired earlier works in the area (as quoted in Ref. 26) is in agreement with Marrucci's theory and with our results. On the other hand, free-rising macroscopic bubbles instantly burst at the surface of fresh water (or by colliding with each other) because the  $\sim 1$  cm/s rise velocities far exceed the critical  $V \sim 100$   $\mu\text{m/s}$  value that follows from our model.

## 5. SUMMARY

We have presented data showing three types of behavior of thin aqueous films between two air bubbles, in the absence of added surfactant. The behavior is shown to depend on approach speed of the bubble surfaces and on electrolyte concentration. The effects of trace surfactants and of evaporation are examined in a companion article.<sup>48</sup>

It is possible to form a stable film in carefully purified water if the bubbles are brought together sufficiently slowly so that hydrodynamic pressures are much less than the capillary pressure and the bubbles do not dimple. The film thickness as a function of capillary pressure matches the disjoining pressure isotherm calculated from DLVO theory with a surface potential of  $-57$  mV on the bubble surfaces. No evidence is found for any "hydrophobic attraction" between bubbles that has been proposed by other authors.<sup>53,54</sup> Even small amounts of electrolyte ( $<1$  mM) destabilise this film. The requirements of very clean water and very careful approach may explain why such films have only rarely been reported.<sup>5</sup>

When the speed of approach is increased slightly ( $\sim 1 - 100$   $\mu\text{m/s}$  for the  $\sim\text{mm}$  radius "bubbles" investigated here) the behavior changes. Films are transiently stable, for periods of  $\sim 10 - 100$  s, but then collapse. Submerged bubbles approaching under such conditions would collide and then rebound if the collision time were less than the film stability time, so bubble coalescence would be inhibited. This behavior can be explained only if the bubble surfaces are effectively immobilised, or partially immobilised, by surface-active solutes giving rise to spatial variations in surface tension. Only small ( $\sim 0.1$  mN/m or less) differences in surface tension are enough to immobilise the bubble surfaces and create hydrodynamic drag sufficient to retard the thin film drainage and cause the transient stability. Surfactant does not need to be added to water for this situation to be possible. Water is never a single-component liquid, and the ions that are inevitably present due to water's self-dissociation could contribute to local variations in surface tension through coupling between flow, deformation, electrostatic, entropic, and electrophoretic effects. Other ions present, even in trace amounts, could also contribute.

The third type of behavior occurs when bubbles approach at higher speeds ( $> \sim 100$   $\mu\text{m/s}$ ). In this case the small surface tension differences possible in purified water are not enough to immobilise the bubble surfaces, and a transition to mobile surfaces occurs. With mobile surfaces, hydrodynamic pressures in the film are much reduced, and the bubbles collide almost instantaneously and without undergoing any observable deformation.

A simple model explaining these three types of behavior has been presented. The model is able to give reasonable estimates of the transition speeds between the observed regimes of behavior in pure water. It can also explain the effects of added electrolyte which essentially kills the low-speed (stable film) and high-speed (rapid coalescence) regimes observed in pure water. More precise predictions will require a more comprehensive model to be developed that includes the effects of surface deformation, coupling between solute convection and diffusion in the film, electrostatic and electrokinetic effects, and adsorption mechanisms and kinetics so that local and instantaneous values of surface tension can be computed.

Bubble coalescence at approach speeds above a fraction of 1 mm/s is consistent with the well-known instability of foams in clean water. The ability of added electrolyte at high concentration to prevent bubble coalescence is consistent with reports in the literature. The present work highlights the significance of bubble approach speeds in determining bubble coalescence, and points to a connection between approach speeds and the transition concentrations at which inorganic electrolytes have been observed to inhibit bubble coalescence.

## Acknowledgments

This work was supported by the Australian Research Council (ARC) Special Research Centre for Particle and Material Interfaces, and Discovery Project DP0986371. Phil Souter (IWR) is gratefully acknowledged for technical assistance as is Tristan Stevens for carrying out support experiments on free-rising bubbles. VY was grateful to the Advanced Technologies Center, Moscow, for its support. EAV appreciates support from the American Chemical Society Petroleum Research Fund Grant #44523-AC5 and the National Institute of Health PHS 1 R01 HL 69965-04. SO acknowledges the ARC for a Queen Elizabeth II Fellowship and research fund DP0343352. We have many people to thank for helpful discussions, and in particular James Beattie, Steve Carnie, Derek Chan, Lorena del Castillo, Marta Krasowska, Stan Miklavcic, John Ralston, and Lee White. The comments of three conscientious reviewers have helped us improve the manuscript.

## APPENDIX 1. CONSIDERATION OF PRESSURES

Pressures at various positions are illustrated in Fig. A1. At the level of the film the hydrostatic pressure is

$$P_G = P_A - \Delta\rho gH, \quad (\text{A1})$$

where  $\Delta\rho$  is the density difference between water and air,  $g$  is the gravitational acceleration, and  $H$  (taken to be positive) is the height difference to the reservoir as shown in Fig. 1. Within the film there may be additional contributions from disjoining pressure  $\Pi$  and hydrodynamic pressure  $P_{hyd}$ , so

$$P_F = P_A - \Delta\rho gH + \Pi + P_{hyd}. \quad (\text{A2})$$

From the Young-Laplace equation, the pressure difference between the film and the surrounding atmosphere is related to the local curvature of the film's surface, which gives

$$P_F(r) = P_A - 2\gamma/R(r) \quad (\text{A3})$$

where  $\gamma$  is interfacial tension,  $2/R$  is the local Gaussian curvature of the film surfaces, and we have emphasized the fact that curvature is in general a function of position  $r$ . In the thicker region of the film near its borders, disjoining pressure and hydrodynamic pressure contributions are negligible, so we have

$$P_B = P_A - 2\gamma/R_B. \quad (\text{A4})$$

Equating (A1) and (A4) for  $P_B$  and  $P_G$  leads to

$$\Delta\rho gH = 2\gamma/R_B, \quad (\text{A5})$$

in which it must be noted that  $2/R_B$  is the Gaussian curvature in the border region, which is not as simple as the 1-D curvature sketched in Fig. A1. Finally, in the case of a static film ( $P_{hyd} =$

0) having a flat region with essentially constant thickness  $h$  over an area of radius  $a$ , the absence of curvature of the surfaces means that  $P_F = P_A$  and therefore from (A2) and (A5),

$$\Pi(h) = \Delta\rho g H = 2\gamma/R_B. \quad (\text{A6})$$

In general,

$$\Pi\{(h(r))\} + P_{\text{hyd}}(h, r) = \Delta\rho g H - 2\gamma/R(r) \quad (\text{A7})$$

at all positions in the film.

There is a pressure head  $H_c$  which is just sufficient to draw the two undistorted menisci (i.e., having radius  $R_c$ ) together. This corresponds to the capillary rise equation

$$\Delta\rho g H_c = 2\gamma/R_c. \quad (\text{A8})$$

We will refer to  $2\gamma/R_c$  as the capillary pressure for the capillary of radius  $R_c$ . A stable film can only be formed for  $H > H_c$  if the sum of disjoining and hydrodynamic pressures exceeds this capillary pressure; if the disjoining pressure alone does not exceed it, only transient stability can be obtained under dynamic conditions, for the period that the hydrodynamic pressure remains sufficiently strong.

## REFERENCES

- Boys, CV. Soap Bubbles. Their Colors and Forces which Mold Them. New York: Dover Publications; 1959.
- Bikerman, JJ. Foams. Vol. v. 10. New York: Springer-Verlag; 1973. Applied Physics and Engineering.
- Exerowa, D.; Kruglyakov, PM. Foam and Foam Films. Theory, Experiment, Application. Amsterdam: Elsevier; 1998. Studies in Interface Sciences series.
- Scheludko A, Exerowa D. Kolloid-Z 1959;165:148.
- Exerowa D. Kolloid-Z 1969;232:703.
- Kolarov T, Yankov R, Esipova NE, Exerowa D, Zorin ZM. Colloid Polym. Sci 1993;271:519.
- McTaggart HA. Phil. Mag 1914;27:297.
- Currie BW, Alty T. Proc. Roy. Soc. London 1929;A122:622.
- Klein O, Lange E. Z. Elektrochemie 1938;44:542.
- Frumkin AN, Iofa ZA, Gerovich MA. Russian Journal of Physical Chemistry. Zh. Fiz. Khim 1956;30:1455.
- Huddleston, RW.; Smith, LA. Foams. Akers, RJ., editor. London: Academic Press; 1976. p. 163-177.
- Usui S, Sasaki H, Matsukawa H. J. Colloid Interface Sci 1981;81:80.
- Graciaa A, Morel G, Saulner P, Lachaise J, Schechter RS. J. Colloid Interface Sci 1995;172:131.
- Marinova KG, Alargova RG, Denkov ND, Velev OD, Petsev DN, Ivanov IB, Borwankar RP. Langmuir 1996;12:2045.
- Karraker KA, Radke CJ. Adv. Colloid Interface Sci 2002;96:231. [PubMed: 11908789]
- Stubenrauch C, von Klitzing R. J. Phys.: Condens. Matter 2003;15:R1197.
- Exerowa D, Churaev NV, Kolarov T, Esipova NE, Panchev N, Zorin ZM. Adv. Colloid Interface Sci 2003;104:1. [PubMed: 12818487]
- Stubenrauch C, Rojas OJ, Schlarmann J, Claesson PM. Langmuir 2004;20:4977. [PubMed: 15984258]
- Ciunel K, Armlin M, Findenegg GH, von Klitzing R. Langmuir 2005;21:4790. [PubMed: 15896011]

20. Claesson PM, Kjellin M, Rojas OJ, Stubenrauch C. *Phys. Chem. Chem. Phys* 2006;8:5501. [PubMed: 17136265]
21. Creux P, Lachaise J, Graciaa A, Beattie JK. *J. Phys. Chem* 2007;111:3753.
22. Beattie JK, Djerdjev AM, Warr GG. *Faraday Discuss* 2009;141:31. [PubMed: 19227349]
23. Parfenyuk VI. *Colloid J* 2002;64:588.
24. Vácha R, Buch V, Milet A, Devlin JP, Jungwirth P. *Phys. Chem. Chem. Phys* 2007;9:4736. [PubMed: 17712453]
25. Pushkarova RA, Horn RG. *Langmuir* 2008;24:8726. [PubMed: 18656971]
26. Marrucci G. *Chem Eng. Sci* 1969;24:979.
27. Lessard RR, Zieminski SA. *Ind Eng. Chem. Fundam* 1971;10:260.
28. Prince MJ, Blanch HW. *AIChE J* 1990;36:1425.
29. Craig VSJ, Ninham BW, Pashley RM. *Nature* 1993;364:317.
30. Christenson HK, Yaminsky VV. *J. Phys. Chem* 1995;99:10420.
31. Craig VSJ. *Curr. Opin. Colloid Interface Sci* 2004;9:178.
32. Henry CL, Dalton CN, Scruton L, Craig VSJ. *J. Phys. Chem. C* 2007;111:1015.
33. Karakashev SI, Nguyen PT, Tsekov R, Hampton MA, Nguyen AV. *Langmuir* 2008;24:11587. [PubMed: 18783259]
34. Christenson HK, Bowen RE, Carlton JA, Denne JRM, Lu Y. *J. Phys. Chem. C* 2008;112:794.
35. Miklavcic SJ. *Phys. Rev. E* 1996;54:6551.
36. Klaseboer E, Chevaillier JP, Gourdon C, Masbernat O. *J. Colloid Interface Sci* 2000;229:274. [PubMed: 10942569]
37. Lin C-Y, Slattery JC. *AIChE J* 1982;28:147.
38. Manica R, Connor JN, Carnie SL, Horn RG, Chan DYC. *Langmuir* 2007;23:626. [PubMed: 17209614]
39. Tambe DE, Sharma MM. *J. Colloid Interface Sci* 1991;147:137.
40. Chen J-D. *J. Colloid Interface Sci* 1984;98:329.
41. Tsekov R, Letocart P, Evstatieva E, Schulze HJ. *Langmuir* 2002;18:5799.
42. Manor O, Vakarelski IU, Tang X, O'Shea SJ, Stevens GW, Grieser F, Dagastine RR, Chan DYC. *Phys. Rev. Lett* 2008;101:024501. [PubMed: 18764184]
43. Bernal JD, Fowler R. *J. Chem. Phys* 1933;1:515.
44. Vogler EA. *Adv. Colloid Interface Sci* 1998;74:69. [PubMed: 9561719]
45. Scriven LE, Sternling CV. *Nature* 1960;187:186.
46. Velarde, MG.; Zeytourian, RK., editors. *Interfacial Phenomena and the Marangoni Effect*. Springer; 2003.
47. Lunkenheimer K, Retter U. *Colloid Polymer Sci* 1993;271:148.
48. Yaminsky VV, Ohnishi S, Vogler EA, Horn RG. submitted to *Langmuir*.
49. Yaminsky VV. *J. Colloid Interface Sci* 2006;297:251. [PubMed: 16297397]
50. Lyklema J, Scholten PC, Mysels KJ. *J. Phys. Chem* 1965;69:116–123.
51. Baszkin A, Nishino M, Ter Minassian-Saraga L. *J. Colloid Interface Sci* 1976;54(3):317–328.
52. Yoon R-H, Aksoy BS. *J. Colloid Interface Sci* 1999;211:1. [PubMed: 9929429]
53. Wang L, Yoon R-H. *Langmuir* 2004;20:11457. [PubMed: 15595770]
54. Nguyen, PT.; Nguyen, AV. *Langmuir*. 2009 Nov 30. published online DOI: 10.1021/la9031333
55. Derjaguin BV, Obukhov E. *Acta Physicochim. URSS* 1936;5:1.
56. Hunter, RJ. *Foundations of Colloid Science*. Oxford: Oxford University Press; 2001.
57. Israelachvili, JN. *Intermolecular and Surface Forces*. 2nd ed.. London: Academic Press; 1991.
58. Hough DB, White LR. *Adv. Colloid Interface Sci* 1980;14:3.
59. Grabbe A. *Langmuir* 1993;9:797.
60. Parsegian VA. *J. Colloid Interface Sci* 1981;81:285.
61. Christenson HK, Claesson PM. *Adv. Colloid Interface Sci* 2001;91:391.
62. Connor JN, Horn RG. *Faraday Discuss* 2003;123:193. [PubMed: 12638862]

63. Connor JN, Horn RG. *Langmuir* 2001;17:7194.
64. Wallqvist V, Claesson PM, Swerin A, Schoelkopf J, Gene PAC. *Langmuir* 2009;25:6909. [PubMed: 19334743]
65. Platikanov D. *J. Phys. Chem* 1964;68:3619.
66. Joye J-L, Miller CA, Hirasaki GJ. *Langmuir* 1992;8:3083.
67. Davis RH, Schonberg JA, Rallison JM. *Phys. Fluids A* 1989;1:77.
68. Abid S, Chesters AK. *Int. J. Multiphase Flow* 1994;20:613.
69. See p.12 of Hardy Sir W, Bircumshaw I. *Proc. Roy. Soc. London* 1925;A108:1.
70. Chan DYC, Horn RG. *J. Chem. Phys* 1985;83:5311.
71. Yiantsios SG, Davis RH. *J. Fluid Mech* 1990;217:547.
72. Chesters AK, Hofman G. *Appl. Sci. Res* 1982;38:353.
73. Radoev VB, Manev E, Ivanov I. *Kolloid Z. Z. Polym* 1969;234:1037.
74. Cain FW, Lee JC. *J. Colloid Interface Sci* 1985;106:70.
75. Connor, JN. PhD thesis. University of South Australia; 2001. Measurement of Interactions between Solid and Fluid Surfaces.
76. Henry CL, Parkinson L, Ralston JR, Craig VSJ. *J. Phys. Chem. C* 2008;112:15094.
77. Parkinson L, Ralston JR. *J. Phys. Chem. C*. 2010 Jan. 15; published online DOI: 10.1021/jp9099754.
78. Horn RG, Asadullah M, Connor JN. *Langmuir* 2006;22:2610. [PubMed: 16519461]
79. Joye J-L, Hirasaki GJ, Miller CA. *Langmuir* 1994;10:3174.
80. Safouane M, Langevin D. *ChemPhysChem* 2009;10:222. [PubMed: 19072821]
81. Kirkpatrick RD, Lockett MJ. *Chem. Eng. Sci* 1974;29:2363.
82. Ribiero CP, Mewes D. *Chem. Eng. J* 2007;126:23.

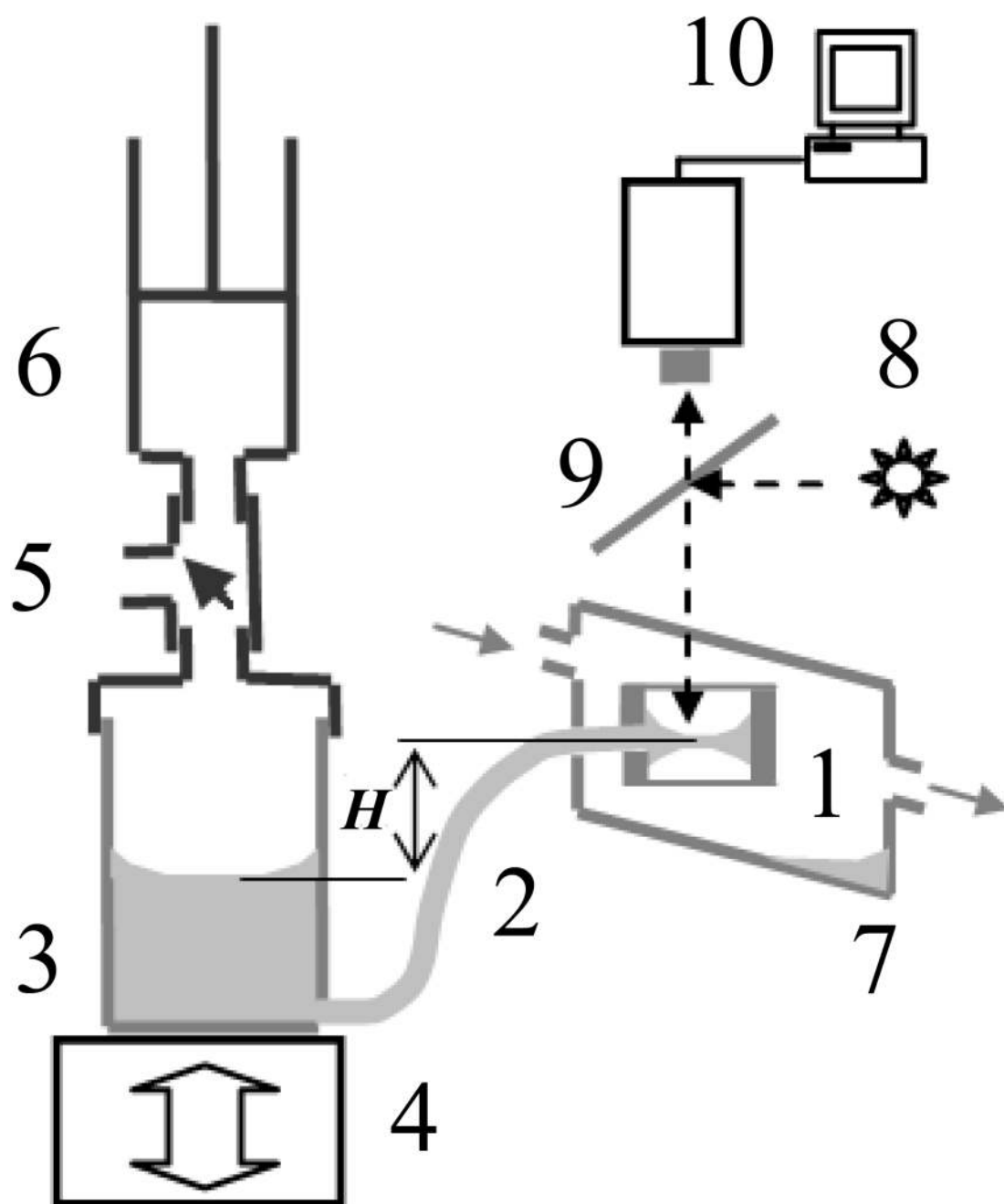


**Figure 1.**

The film balance: 1 – film holder, 2 – flexing tube, 3 – communication vessel, 4 – drive, 5 – three-way valve, 6 – syringe, 7 – vapor/flow cell, 8 – light source, 9 – beam splitter, 10 – videomicroscope

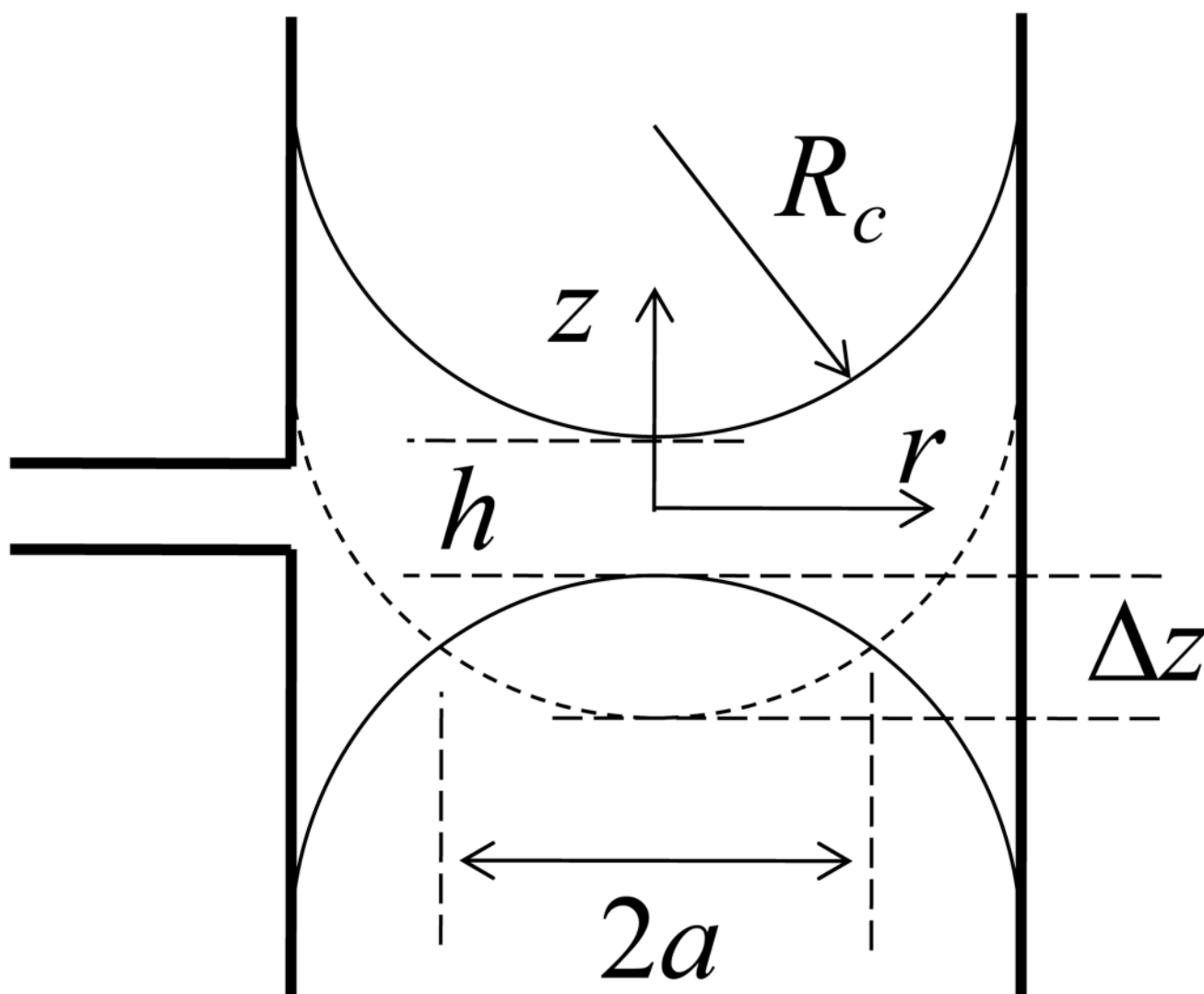


**Figure 2.** Undistorted meniscus geometry. (The dotted hemisphere and displacement  $\Delta z$  are to assist with discussion of Fig. 5.)

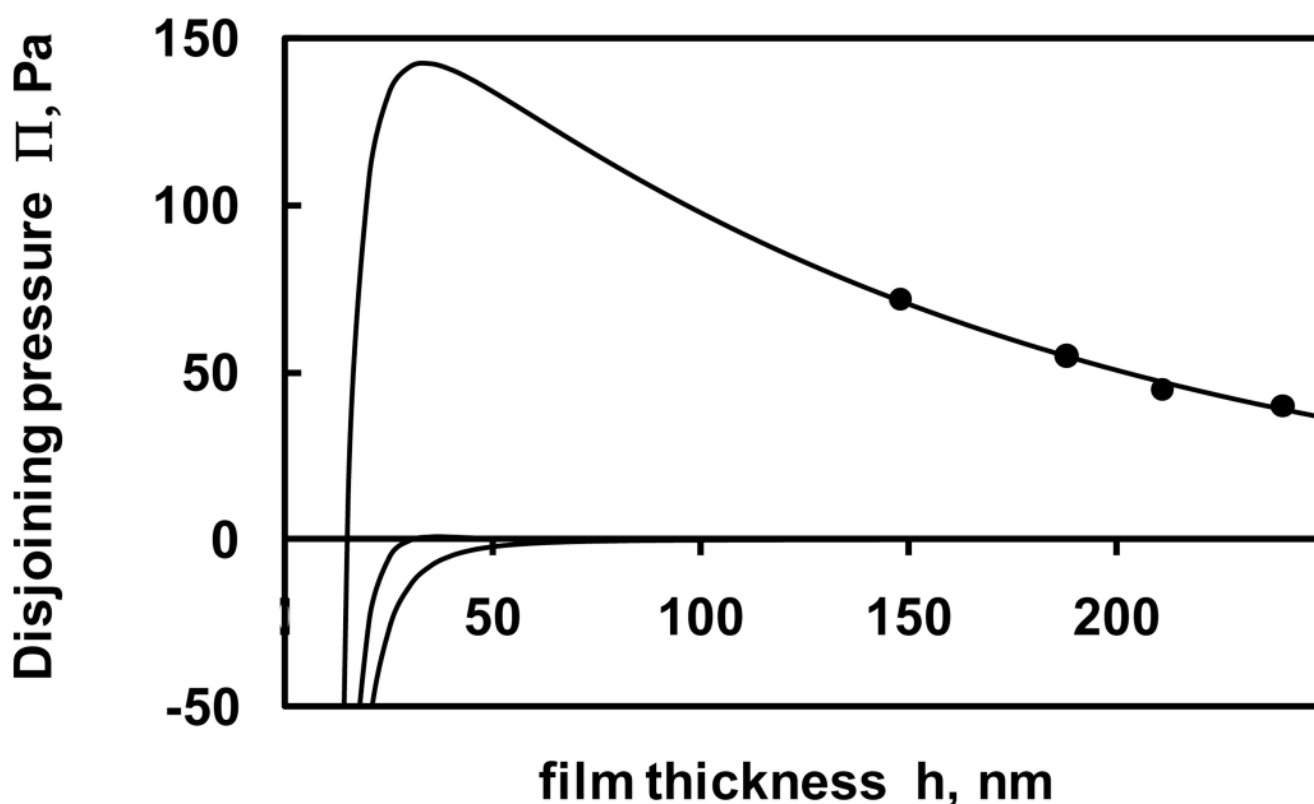


**Figure 3.**

Measured pressure in a flattened film of distilled water as a function of film thickness (solid circles). This measurement was done using a 4.3 mm diameter ring. Cyclic measurements show repeatability, with no hysteresis. The magnitude and decay length of the isotherm slowly change on long time scales, and can vary between experiments due to concentration variations of background electrolyte and ingress of trace surface impurities. The solid line shows DLVO disjoining pressure calculated between two air phases interacting across a thin aqueous film with 4  $\mu\text{M}$  electrolyte (i.e., near-pure water) giving a Debye length of 152 nm. The fitted surface charge has magnitude 0.32  $\text{mC}/\text{m}^2$ , which corresponds to a surface potential of magnitude 57 mV. The dashed line shows a calculation for the same surface charge and 0.8 mM electrolyte, while the dotted line shows the van der Waals component only (see Fig. 4).

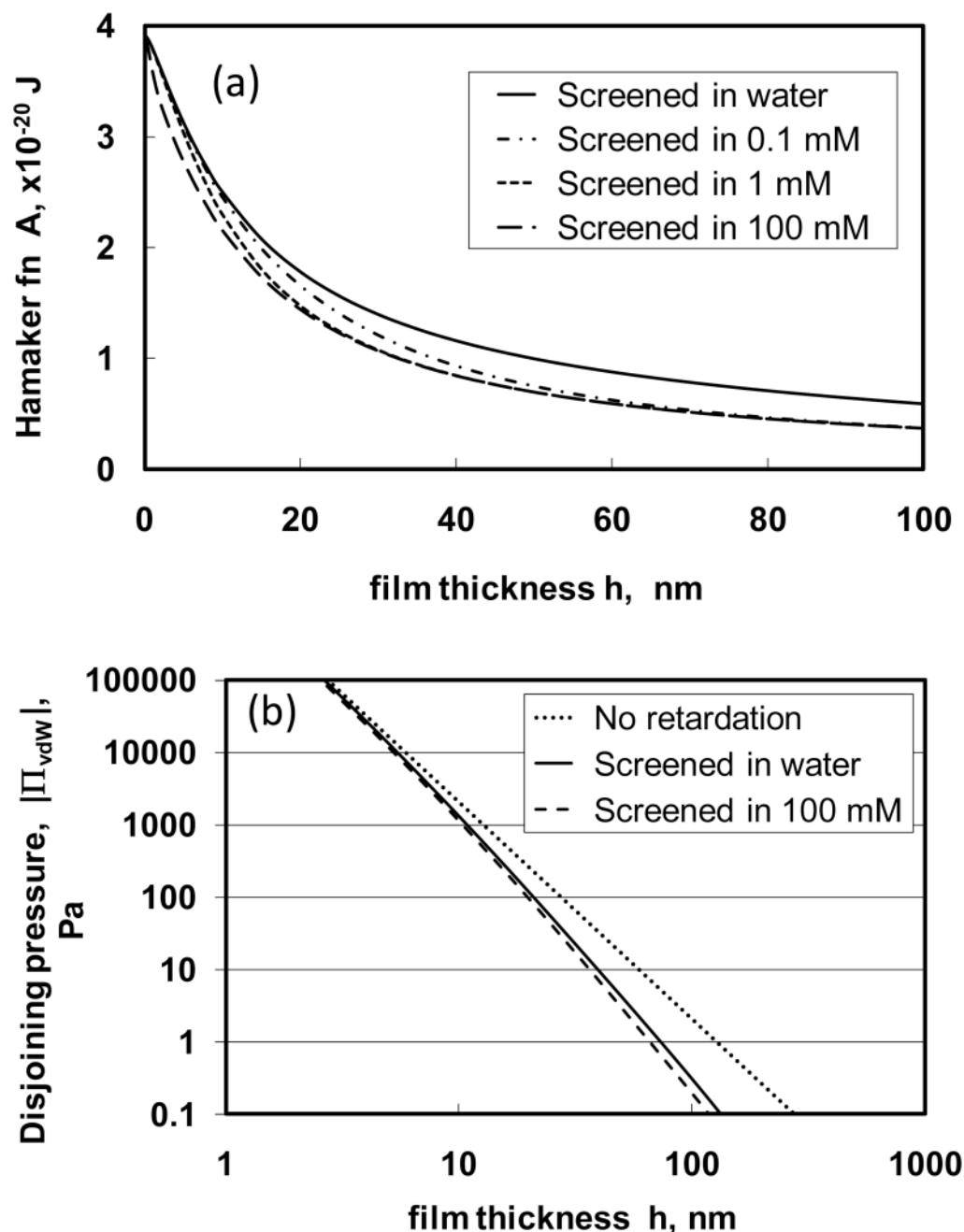


**Figure 4.**

(a) The Hamaker function calculated for vacuum/water/vacuum from the Lifshitz theory, as programmed by Grabbe59 using the representation of Parsegian60 for the dielectric properties of water. The four curves correspond to four different screening lengths for the zero-frequency component of the Hamaker function, corresponding to four concentrations of monovalent electrolyte: near-pure water ( $4 \mu\text{M}$ ) (solid line);  $0.1 \text{ mM}$  (dash-dotted);  $1 \text{ mM}$  (dotted) and  $100 \text{ mM}$  (dashed). (b) the magnitude of the (negative) van der Waals component of disjoining pressure  $\Pi_{\text{vdW}}$  as a function of aqueous film thickness  $h$  plotted on a log-log scale for two electrolyte concentrations,  $4 \mu\text{M}$  (solid line) and  $100 \text{ mM}$  (dashed line). The non-retarded form ( $A = 3.9 \times 10^{-20} \text{ J}$ ) is also shown for comparison (dotted line).

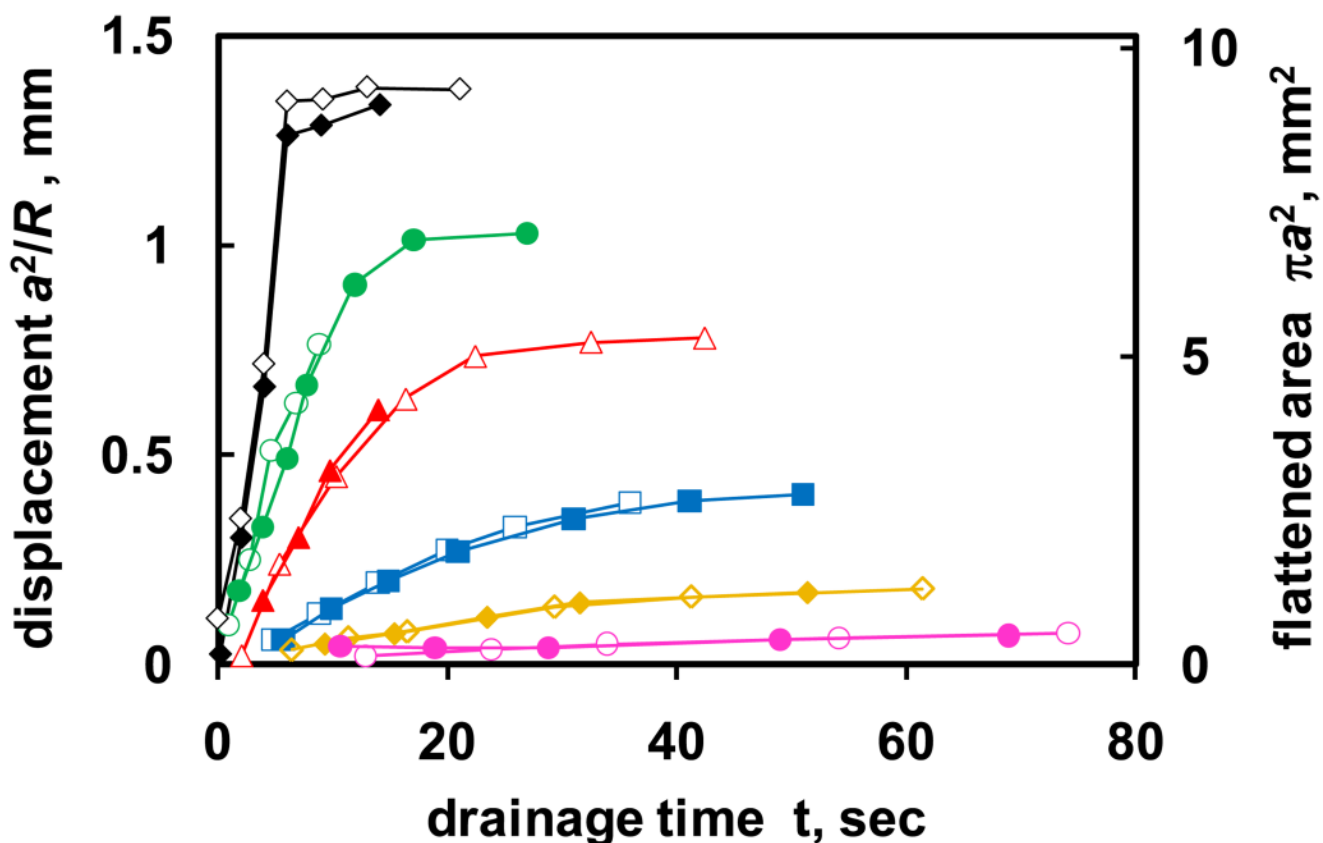


**Figure 5.**

The film area expansion in free drainage from different heights  $H$ : 1 mm (magenta circles), 1.7 mm (orange diamonds), 3.2 mm (blue squares), 6.4 mm (red triangles), 10 mm (green circles), and 20.4 mm (black diamonds), in the sequence of curves from bottom to top. Two sets of measurements at each speed are shown, indicated by filled and hollow symbols. The last point of each measurement is immediately before the film breaks. Note that as long as measured radius  $a$  of the film remains much smaller than the meniscus radius  $R$ , the term  $a^2/R$  equals displacement of the meniscus surfaces in the  $z$  direction of mutual approach (see Fig. 2). The speed of mutual approach of the surfaces before the film starts forming is thus the initial slope of the curves. The drainage rate under essentially constant pressure difference scales with  $H$  and with hydrodynamic resistance of the communication path.

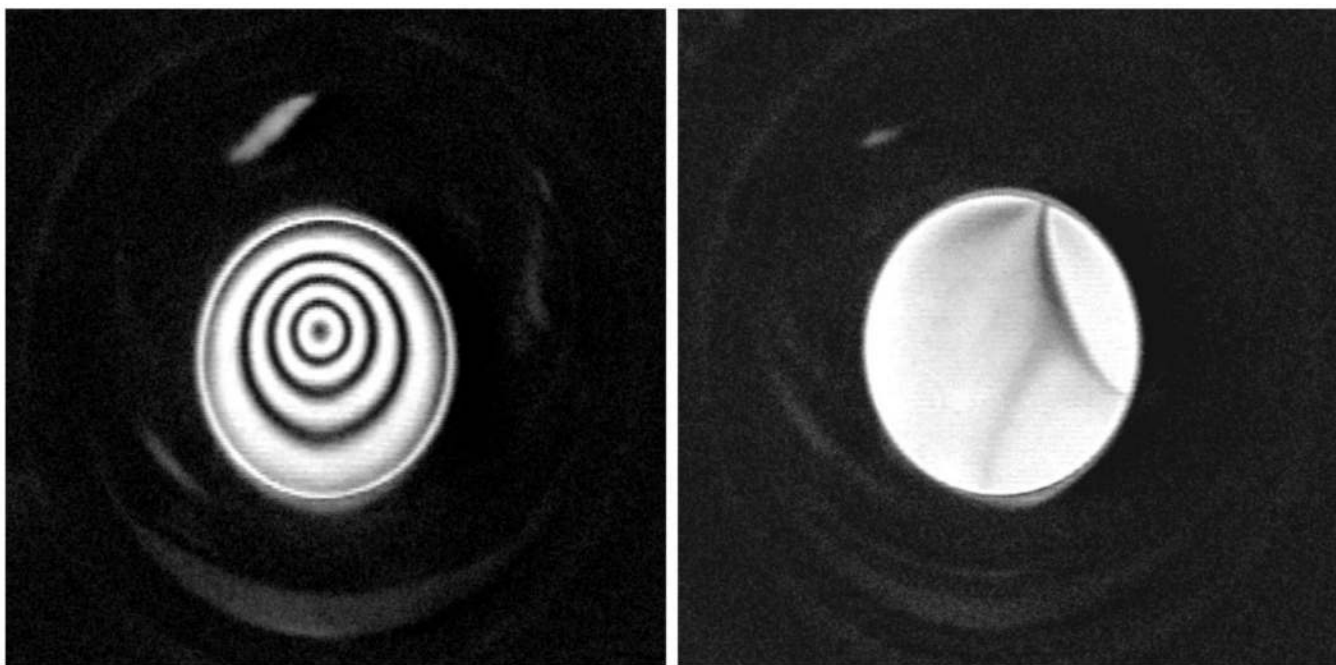


**Figure 6.**

(a) A dimple observed in a transient film of water at approach speed  $V = 150 \mu\text{m/s}$  (which is below the transition speed in this particular experiment). (b) Wedge draining observed in a transient film of 1 mM NaCl aqueous solution ( $V = 5 \mu\text{m/s}$ ) (Section 3.2.4). Similar features are also observed in water films, but those eventually reach uniform thickness. The transient salt solution film drains and then ruptures at its thinnest point without becoming uniform. Both film radii are 1 mm.

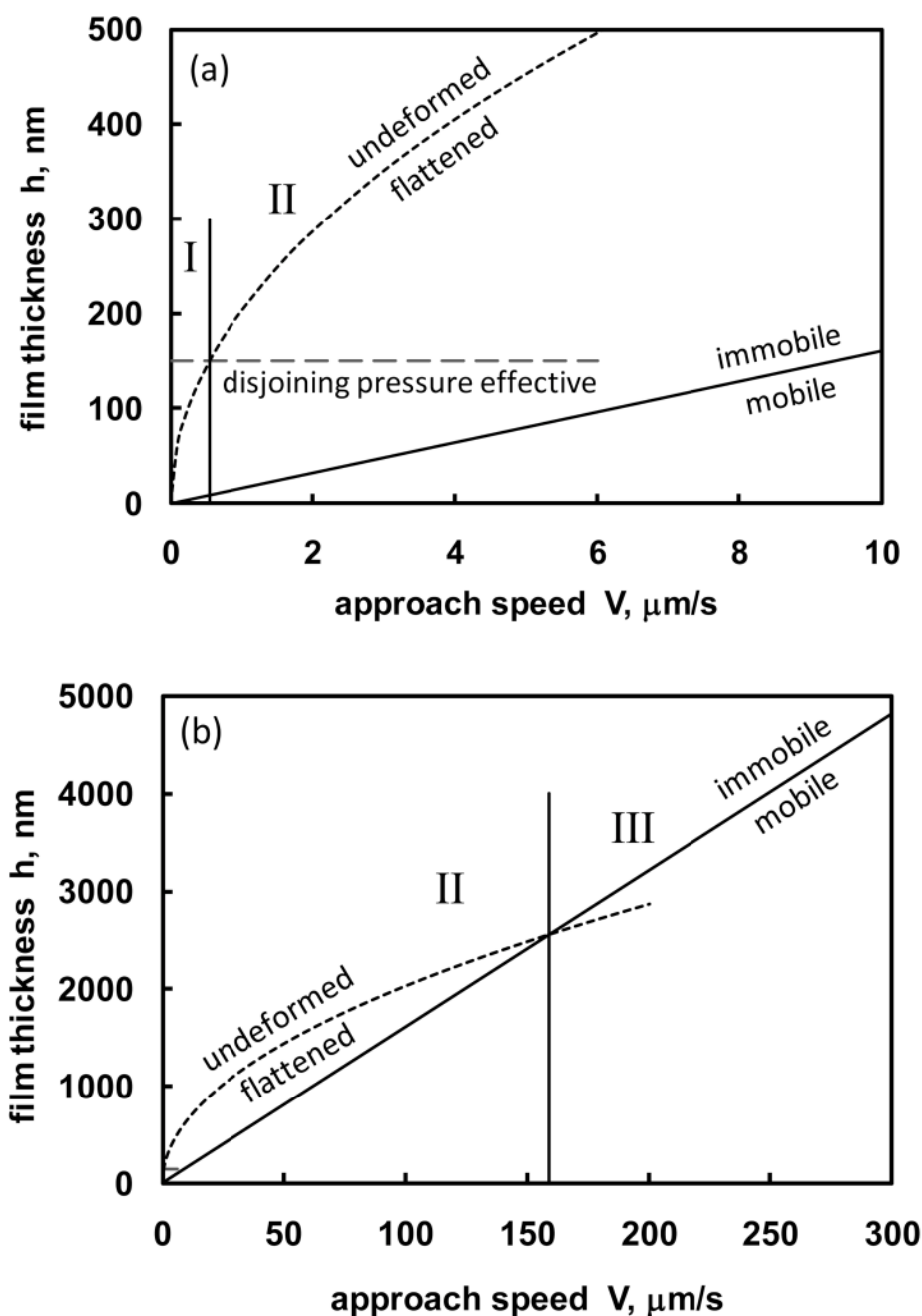


**Figure 7.**

Illustration of the different regimes of behavior depending on the approach speed of two bubbles, plotted on two different scales. The continuous lines show the demarcation between immobile and mobile bubble surfaces according to Eqn. (10), with a value of  $0.07 \text{ mN/m}$  chosen for the parameter  $\Delta\gamma$ . Dotted lines show the thickness at which flattening occurs as a function of approach speed, according to Eqn. (9) (which is only valid in the immobile region), using parameters appropriate for bubbles approaching in water. Part (a) shows the curves for lower approach speeds, and includes a horizontal dashed line to indicate the effective range of disjoining pressure in distilled water. Regions I (stable film, i.e., no coalescence); II (transient

film, delayed coalescence); and III (no film, instant coalescence) are discussed in Section 5 of the text.

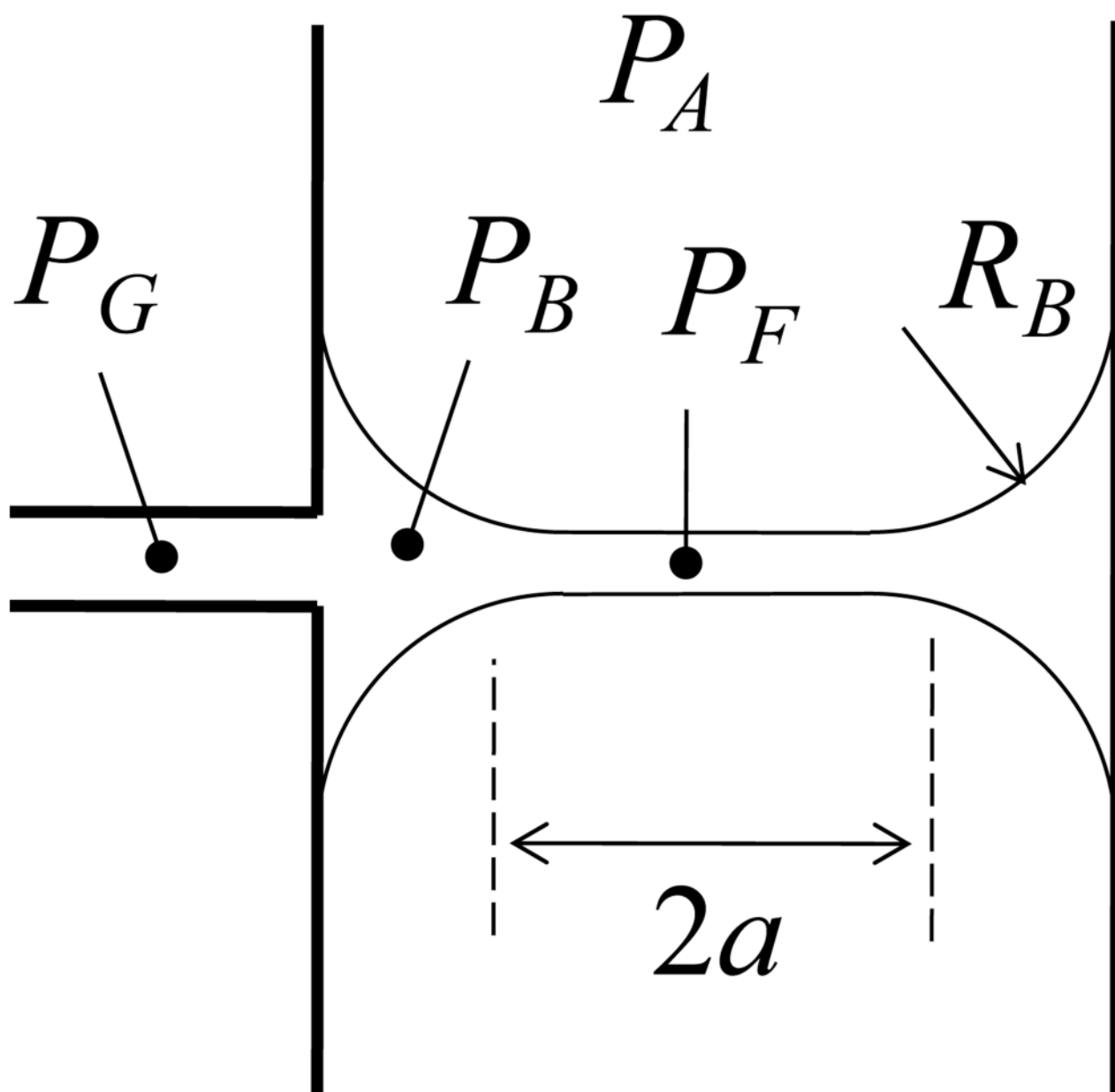


**Figure A1.**  
Diagram indicating pressures at various locations in the film balance.

**Table 1**

Features of films at various approach speeds (under vapor saturation)

Film media	distilled water	NaCl aqueous solution concentration	
Approach speed, $dh/dt$		0.8 mM–100 mM	>100 mM
$dh/dt < 1 \mu\text{m/s}$	Stable film (optically uniform) *	No film	No film
$1 \mu\text{m/s} < dh/dt < \text{critical speed of water film (100–200 } \mu\text{m/s)}$	Transient film (dimple and subsequent chaotic draining)	Transient film (wedge draining and asymmetric thinning)	No film or transient film as approaching speed increases
$dh/dt > \text{critical speed of water film (100–200 } \mu\text{m/s)}$	No film (instant coalescence)	No film or transient film as concentration increases	Continuous film (vortex, dimple, chaotic flow)

Note: The lifetimes of stable films and continuous films are more than several minutes. The lifetime of transient films is about a minute or less.

\* Stable film was observed up to 0.1 mM NaCl, and marginal stability sometimes observed at concentrations between 0.1 and 0.5 mM. Above 0.8 mM, films were never stable.